[J] Poster | S (Solid Earth Sciences) | S-SS Seismology

[S-SS10] Fault Rheology and Earthquake Physics

convener:Ritsuya Shibata(National Research Institute for Earth Science and Disaster Resilience), Michiyo Sawai(Chiba University), Hanaya Okuda(Kochi Institute for Core Sample Research, Japan Agency for Marine-Earth Science and Technology), Kenichi Tsuda(Institute of Technology, Shimizu Corporation)
Fri. May 30, 2025 5:15 PM - 7:15 PM Poster Hall (Exhibition Hall 7&8, Makuhari Messe)
The goal of this session is to integrate theoretical, experimental, observational, and numerical perspectives from various fields such as seismology, geodesy, geology, mineralogy, and so on, to define what is known about earthquake source processes and the physical and chemical elementary processes of faulting. This session welcomes studies that address such issues as pre-, co-, and post-seismic processes, the rheology of seismogenic faults and fault rocks, laboratory experiments on elementary processes, numerical models based on frictional laws, and estimates of the stress field in the seismogenic zones. We also welcome studies on fault-zone drilling projects and in situ stress measurements.

[SSS10-P01] Spontaneous crack tip propagation outside the nucleation zone taking account of the rate-and-state friction law and the interaction between heat and fluid

*Yoko Kono[1], Takehito Suzuki[2] (1.Aoyama Gakuin University, 2.Takachiho univ.)
5:15 PM - 7:15 PM

[SSS10-P02] Investigation of the Physical Mechanism of Adjacent Slow and Repeating Earthquakes Using a Wavy Frictional Heterogeneity Model

*Yuki Watanabe[1,2], Yuta Mitsui[1] (1.Shizuoka University, 2.Currently at Kyoto University, Graduate School)
5:15 PM - 7:15 PM

[SSS10-P03] Unexpected rupture triggering behavior of subshear and free-surface-induced supershear ruptures on stepover: which is more dangerous?

*Zijia Wang[1], Zhenguo Zhang[1] (1.Department of Earth and Space Sciences, Southern University of Science and Technology)
5:15 PM - 7:15 PM

[SSS10-P04] Influence of the Shallow Low-Velocity Layer on Fault Rupture Behavior Using a Dynamic Model

*Shotaro Tane[1], Naoki Iwata[1], Kenichi Tsuda[2], Junichi miyakoshi[2] (1.Chuden Engineering Consultants Co., Ltd, 2.Shimizu Corporation)
5:15 PM - 7:15 PM

[SSS10-P05] Fault Rupture Termination of the 2016 Kumamoto earthquake within Aso Caldera: Insights from Multi-Beam Back-Projection and Strong Motion Records

*Nelson Pulido[1] (1.National Research Institute for Earth Science and Disaster Resilience)
5:15 PM - 7:15 PM

[SSS10-P06] Dynamic Rupture Inversion of Finite-fault with Curved Grid Finite-Difference Method: Synthetic Test and Applications

*Yuchen Zhang[1], Zhenguo Zhang[1], Zhongqiu He[1] (1. Department of Earth and Space Sciences, Southern University of Science and Technology, Shenzhen 518055, China)

5:15 PM - 7:15 PM

[SSS10-P07] Analytical approaches for simultaneous inversion of distributed slip, Green's function, and fault geometry

*Daisuke Sato[1], Yuji Yagi[2], Ryo Okuwaki[2], Yukitoshi Fukahata[3] (1.Japan Agency for Marine-Earth Science and Technology, 2.Tsukuba University, 3.Disaster Prevention Research Institute, Kyoto University)

5:15 PM - 7:15 PM

[SSS10-P08] Deconvolution Approach to Estimate Radiation Process of Large (Mw7.0-9.0) Earthquakes

*Keisuke Yoshida[1] (1.Tohoku University)

5:15 PM - 7:15 PM

[SSS10-P09] Analysis of Source Characteristics of Earthquakes Potentially Induced by Wastewater Injection in Peace River, Alberta, Canada

Koki Kamata[1], *Ahyi KIM[1], Jeffrey Gu[2], Wenhan Sun[2], Tai-Chieh Yu[2] (1.Yokohama City University, 2.University of Alberta)

5:15 PM - 7:15 PM

[SSS10-P10] Reproduction of interplate slip phenomena along the Nankai Trough: Deep short-term slow slip events

*Fuyuki Hirose[1] (1.Seismology and Tsunami Research Department, Meteorological Research Institute)

5:15 PM - 7:15 PM

[SSS10-P11] Relationship between the Boso slow slip events and the accompanying earthquake swarm: Part 2

*Issei Yasuhara[1], Toshinori Sato[2] (1.Graduate School of Science and Engineering, Chiba University, 2.Graduate School of Science, Chiba University)

5:15 PM - 7:15 PM

[SSS10-P12] High-resolution estimation of the Boso Slow Slip Events in 2011, 2013–2014, 2018, and 2024 based on inflection point analysis of high-rate GNSS data

*Yuta Mitsui[1], Riko Arai[1], Shiori Watanabe[1,2] (1.Shizuoka Univ., 2.Univ. of Tsukuba (currently))

5:15 PM - 7:15 PM

[SSS10-P13] Mapping Fault Zone Attenuation Using MiDAS Downhole Optical Fiber and Borehole Seismic Arrays

*Lu Hsiao[1], Kuo-Fong Ma[1,2], Yen-Yu Lin[1] (1.Institute of Geophysics, National Central University, 2.Institute of Earth Sciences, Academia Sinica)

5:15 PM - 7:15 PM

[SSS10-P14] Calcite-bearing cataclasite and non-double-couple earthquakes in the aftershock area of the 2000 Tottori-ken Seibu earthquake

*Kiyokazu Oohashi[1], Kenta Kobayashi[2] (1.National Institute of Advanced Industrial Science and Technology , 2.Department of Geology, Faculty of Science, Niigata University)

5:15 PM - 7:15 PM

[SSS10-P15] Seismic Fault Repetition Estimated from Pseudotachylyte in Eidsfjord, Northern Norway

*Asuka Tsuda[1], Takamoto Okudaira[1] （1.Osaka Metropolitan University）
5:15 PM - 7:15 PM

[SSS10-P16] Evaluation of fluidization during earthquake slip at the primary slip zone in the Neogene accretionary complex, Boso Peninsula, Japan

*Tatsuru Fukuta[1], Tetsuro Hirono[1] （1.Osaka Metropolitan Univercity）
5:15 PM - 7:15 PM

[SSS10-P17] Quantitative evaluation of surface fracture energy in minor fault adjacent to the Taiwan Chelungpu fault

*Takumi Kawakami[1], Tetsuro Hirono[1] （1.Osaka Metropolitan University）
5:15 PM - 7:15 PM

[SSS10-P18] Investigating Smectite Content in Neodani Fault Gouge: A Quantitative Approach to Understanding of Fault Mechanics

*Bosco de Sousa Auxilio[1], Tomoyuki Ohtani[1] （1.Gifu Univ.）
5:15 PM - 7:15 PM

[SSS10-P19] Relationship between deformation structure and seismic slip in the shallow part of the Neodani Fault zone

*Tsuyoshi Maeda[1], Tomoyuki Ohtani[2] （1.Gifu University Graduate School of Natural Science and Technology, 2.Faculty of Engineering, Gifu University ）
5:15 PM - 7:15 PM

[SSS10-P20] Off-fault Damage Development as Revealed by Fault Surveys

*Kosei Ogita[1], Jun Muto[1], Hiroyuki Nagahama[1], Sando Sawa[1] （1.TOHOKU UNIVERSITY）
5:15 PM - 7:15 PM

[SSS10-P21] Deformation mechanisms of quartz in plate boundary rocks deformed in a deep slow earthquake source region

*Shota Komagino[1], Kohtaro Ujiie[1], Thomas Yeo[1], Norio Shigematsu[2] （1.University of Tsukuba, 2.National Institute of Advanced Industrial Science and Technology）
5:15 PM - 7:15 PM

[SSS10-P22] Shear zone development in the deep part of subduction zone recorded in the Kerama Islands, Okinawa

*Kei Takahashi[1], Asuka Yamaguchi[1], Makoto Otsubo[2] （1.The University of Tokyo, 2.National Institute of Advanced Industrial Science and Technology）
5:15 PM - 7:15 PM

[SSS10-P23] Deformation mechanisms and stress field induced by seamount subduction: A case study at Funafuseyama Unit, Mino belt

*Fuka Takuwa[1], Asuka Yamaguchi[1], Makoto Otsubo[2], Yusuke Shimura[2], Hanaya Okuda[3] （1.The University of Tokyo, 2.National Institute of Advanced Industrial Science and Technology, 3.Kochi Institute for Core Sample Research, Japan Agency for Marine-Earth Science and Technology）
5:15 PM - 7:15 PM

[SSS10-P24] Frictional properties of limestone from seamounts under high temperature and high pressure

*Mayuko Sekikawa[1], Hanaya Okuda[2], Manami Kitamura[3], Miki Takahashi[3], Asuka Yamaguchi[4], Michiyo Sawai[1] （1.Chiba University, 2.Kochi Institute for Core Sample Research, Japan Agency for Marine-Earth Science and Technology, 3.National Institute of Advanced Industrial Science and Technology, 4.Atmosphere and Ocean Research

Institute, The University of Tokyo)
5:15 PM - 7:15 PM

[SSS10-P25] Experimental investigation on effects of diagenesis on frictional and hydraulic properties of incoming sediments from Tohoku subduction zone
*Hayato Ito[1,2], Keishi Okazaki[1,2], Mizuki Ueda[1,3], Asuka Yamaguchi[4], Yohei Hamada[2] (1.Hiroshima University, 2.Kochi Institute for Core Sample Research, JAMSTEC, 3.University of Tsukuba, 4.AORI, The University of Tokyo)
5:15 PM - 7:15 PM

[SSS10-P26] Preliminary results of shear friction experiments using Shirahama sandstone for the construction of friction wear model
*Sumire Maeda[1], Futoshi Yamashita[2] (1.National Institute of Advanced Industrial Science and Technology, 2.National Research Institute for Earth Science and Disaster Resilience)
5:15 PM - 7:15 PM

[SSS10-P27] Examination of development process of boundary shear in powdered quartz gouge by rotary-friction experiments
*Minoru Kudose[1], Tetsuro Hirono[1], Hatanaka Mamoru[2], Akito Tsutsumi[2], Takeshi Miyamoto[2], Satoshi Yukawa[3] (1.Osaka Metropolitan University, 2.Kyoto University, 3.Osaka University)
5:15 PM - 7:15 PM

[SSS10-P28] Experimental evaluation of friction property of unaltered and altered basalt
*Yohei Donga[1], Minoru Kudose[1], Akito Tsutsumi[2], Tetsuro Hirono[1] (1.Osaka Metropolitan University, 2.Kyoto University)
5:15 PM - 7:15 PM

[SSS10-P29] Frictional behavior of cation-exchanged biotite
*Hanaya Okuda[1], Akiko Yamaguchi[2] (1.Kochi Institute for Core Sample Research, Japan Agency for Marine-Earth Science and Technology, 2.Center for Computational Science and e-Systems, Japan Atomic Energy Agency)
5:15 PM - 7:15 PM

[SSS10-P30] Dependence of the rate- and state-dependent friction parameters of metagabbro gouge on normal stress
*Futoshi Yamashita[1], Kazuo Mizoguchi[2], Eiichi Fukuyama[3,1], Sachiko Iizuka[4] (1.National Research Institute for Earth Science and Disaster Resilience, 2.CRIEPI, 3.Graduate School of Engineering, Kyoto University, 4.CERES Inc.)
5:15 PM - 7:15 PM

[SSS10-P31] Effects of pore fluid pressurization rate and permeability due to friction surface roughness on friction behaviors
*RIKU IWATA[1], SINICHI UEHARA[1] (1.TOHO university)
5:15 PM - 7:15 PM

[SSS10-P32] Investigating Fracture Mechanisms in Hydraulic Fracturing by Dynamic Event Localization
*Zhi Yuan[1], Chen Gu[1], Yichen Zhong[1], Peng Wu[1], Zhuoyu Chen[1] (1.Tsinghua University)
5:15 PM - 7:15 PM

[SSS10-P33] Toward frictional experiments at brittle-plastic transition pressures with high-flux synchrotron X-ray

*Rikuto Honda[1], Tomoaki Kubo[1], Noriyoshi Tsujino[2], Yuji Higo[2], Sho Kakizawa[2], Sanae Koizumi[3], Yuta Goto[1] （1.Kyushu University, 2.JASRI, 3.The University of Tokyo）

5:15 PM - 7:15 PM

[SSS10-P34] Earthquake Stress-Drop Estimation in Laboratory Experiment with Machine Learning

*Gauss Te-Chuan Chang[1,2], Chris Marone[3,4], Chun-Yu Ke[2] （1.Department of Physics, National Taiwan University, Taipei, Taiwan, 2.Department of Civil Engineering, National Taiwan University, Taipei, Taiwan, 3.Department of Earth Sciences, La Sapienza Università di Roma, Roma, Italy, 4.Department of Geosciences, Pennsylvania State University, PA, USA）

5:15 PM - 7:15 PM

Spontaneous crack tip propagation outside the nucleation zone taking account of the rate-and-state friction law and the interaction between heat and fluid

*Yoko Kono[1], Takehito Suzuki[2]

1. Aoyama Gakuin University, 2. Takachiho univ.

The propagation velocity of fault tips and nucleation mechanism of cracks have attracted interests of researchers. For example, Suzuki and Yamashita (2009, JGR) simulated the propagation of crack tips by incorporating the effects of the interaction among heat, fluid, and pore generation. This model successfully explains both the fast and slow earthquakes. However, note that Suzuki and Yamashita (2009) used a simple friction coefficient consisting of a constant static friction coefficient and a kinetic friction coefficient. Recent studies have suggested that a rate-and-state dependent friction law is a more appropriate friction law. The rate-and-state-dependent friction law characterizes the effect of the slip velocity on the friction coefficient and the effect of the state variables with the parameters A and B, respectively. It should be noted that the larger A-B induces the stronger velocity strengthening. Moreover, they did not treat tremors.
In the current study, the rate-and-state-dependent friction law and the interaction between the heat and fluid are incorporated in a single framework. Spontaneous crack propagation in a two-dimensional anti-plane shear crack is considered. We consider the slip zone whose thickness is w_h, where the heat and fluid effects work. In addition, we consider a nucleation zone, within which the crack tip is assumed to grow at a constant propagation speed. After the crack tip reaches the edge of the nucleation zone, spontaneous propagation begins. In this model, we investigated whether a crack propagates spontaneously or nor by changing the parameters of the rate-and-state-dependent friction law and w_h.
The results of the numerical calculations suggest that when the value of w_h is fixed, propagation outside the nucleation zone occurs when the A-B value is in small and large regions, and does not occur in the intermediate region. Furthermore, it was found that the time when the propagation occurs differs between the small and large A-B groups. In the small A-B group, the propagation begins relatively soon after the crack tip reaches the edge of the nucleation zone, and the larger A-B, the later the propagation occurred. However, in the large A-B group, the propagation exhibits a delay in initiation after the crack tip reaches the edge of the nucleation zone. Additionally, the larger A-B, the earlier the propagation occurred.
We investigate the reason for the difference in the behavior between small and large A-B groups. For the small A-B group, the system behavior is easy to understand. Since the velocity strengthening is weaker for the smaller A-B value, the slip velocity inside the nucleation zone is smaller for larger A-B, and the stress concentration is also smaller for larger A-B. Consequently, the later propagation emerges for the larger A-B value, which is intuitively reasonable. However, the system behaves contrary to intuition for large A-B group. For this group, we first emphasize that the slip velocity inside the nucleation zone is smaller for larger A-B value before the reflected waves arrive on the point. After the reflected waves pass, the slip velocity can become larger for the larger A-B value because the deceleration effect due to the rate-and-state friction law is weaker for the larger A-B. We then note that the heat and fluid effects work inside the nucleation zone during the slip, and the effect can completely release the stress on the crack plane eventually. This effect can emerge earlier for larger A-B, since the slip velocity after the reflected waves pass the point is larger. This induces the earlier stress concentration and earlier propagation outside the nucleation zone.
The result obtained here implies that we should consider both the rate-and-state friction law and the

interaction between heat and fluid to investigate the dynamic earthquake source process. This may provide important insights also for the mechanisms of slow earthquakes such as tremors.

Keywords: heat, fluid, rate-and-state friction law, crack tip propagation, nucleation zone

Investigation of the Physical Mechanism of Adjacent Slow and Repeating Earthquakes Using a Wavy Frictional Heterogeneity Model

*Yuki Watanabe[1,2], Yuta Mitsui[1]

1. Shizuoka University, 2. Currently at Kyoto University, Graduate School

Seismological and geological approaches suggest that friction is heterogeneously distributed on the fault plane. As an example, Yabe and Ide (2018) investigated the effects of frictional heterogeneity on seismicity by setting velocity-strengthening and velocity-weakening patches based on the a-b values of the rate- and state-dependent friction (RSF) law. They configured frictional heterogeneity by alternately placing these patches and conducted earthquake cycle simulations. Their results demonstrated that varying the degree of frictional heterogeneity could reproduce diverse seismicity, indicating that regional differences in seismicity may depend on the characteristics of frictional heterogeneity.
This study assumes frictional heterogeneity and attempts to model the phenomenon in which slow earthquakes and (repeating) earthquakes occur in nearly the same location due to the influence of aseismic slip (e.g., Todd et al., 2018; Takahashi et al., 2022). In addition to the conventional bimodal frictional properties, where the a-b value within each patch is constant, we also examine a wavy frictional property, where the a-b distribution is given by a sine function. This wavy frictional property is a model that accounts for the transient variation of frictional properties due to factors such as pore fluid pressure and mineral composition changes. Furthermore, to clarify the impact of aseismic slip occurring in the velocity-strengthening regions between velocity-weakening patches, the individual velocity-weakening patches were set to be smaller than the critical nucleation size (the minimum patch size required for spontaneous seismic fast slip).
Under these conditions, we performed two-dimensional in-plane earthquake cycle simulations, including dynamic terms, following the methodology of Lapusta et al. (2000). When the interaction between velocity-weakening patches was weak, spontaneous events (tentatively referred to as slow earthquakes) frequently occurred, which did not lead to seismic fast slip, as expected from the critical nucleation size setting. However, when the interaction between velocity-weakening patches was strong, particularly in the wavy frictional heterogeneity model, aseismic slip in the velocity-strengthening regions between velocity-weakening patches often led to stress accumulation on the velocity-weakening patches. In such cases, local acceleration occurred on the velocity-weakening patches where slow earthquakes typically occur, leading to the triggering of seismic fast slip.
In our model, the distinction between slow and seismic fast slip events occurring within the same velocity-weakening patch arises from aseismic slip in adjacent velocity-strengthening regions, highlighting the essential role of frictional heterogeneity. This study proposes a physical mechanism that may explain the closely located tremor and (repeating) earthquake occurrences reported in the shallow subduction zones offshore of New Zealand and Northeastern Japan.

Keywords: Frictional heterogeneity, Rate- and state-dependent friction (RSF) law, Spectral boundary integral equation method, Slow earthquakes, Repeating earthquakes, Tremors

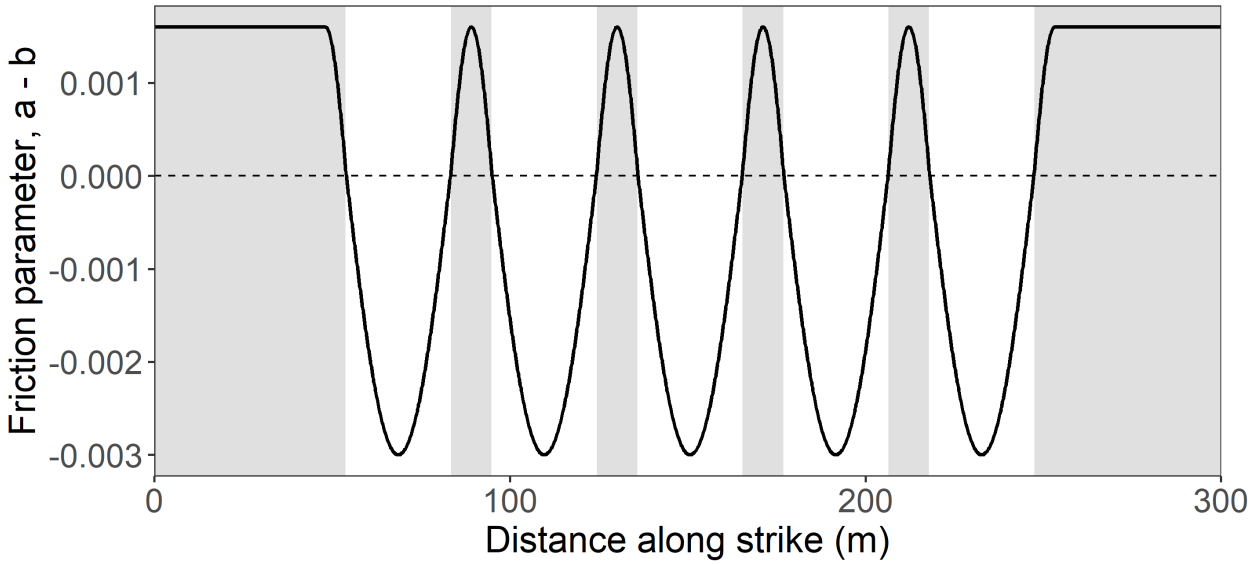

Unexpected rupture triggering behavior of subshear and free-surface-induced supershear ruptures on stepover: which is more dangerous?

*Zijia Wang[1], Zhenguo Zhang[1]

1. Department of Earth and Space Sciences, Southern University of Science and Technology

The ability of a rupture to propagate across a stepover plays a critical role in determining the earthquake’ s final magnitude and potential damage. This study systematically investigated the jump distances of 3D strike-slip faults based on the rate- and state-dependent friction law with strong rate weakening. We found that the jump distances for extensional and compressional steps can reach 5.45 km and 4.5 km, respectively. Moreover, we compared the rupture triggering behavior of subshear and free-surface-induced (FSI) supershear ruptures on the secondary fault. Unexpectedly, both simple and barrier models have demonstrated that, compared to FSI supershear rupture, subshear rupture can result in a larger jump distance for the compressional step due to its stronger dynamic stress perturbation. The free surface also plays an important role in this process. Due to the different stress disturbance modes, the triggering ability on the extensional step does not increase. However, when considering the rate-strengthening layer and depth-dependent stresses, subshear rupture also shows a stronger triggering ability for the extensional step. Our findings were further confirmed by models with different overlap distances. These results emphasize the high cascading rupture potential of subshear ruptures and provide important insights for assessing seismic hazards of multi-fault systems.

Keywords: Strike-slip stepover, Dynamic stress, Rupture triggering, Jump distance, Subshear rupture, Free-surface-induced supershear

Influence of the Shallow Low-Velocity Layer on Fault Rupture Behavior Using a Dynamic Model

*Shotaro Tane[1], Naoki Iwata[1], Kenichi Tsuda[2], Junichi miyakoshi[2]

1. Chuden Engineering Consultants Co., Ltd, 2. Shimizu Corporation

The simulation for dynamic rupture propagation that is based on the force balance is very useful approach to understand the fault behavior especially to the shallow part of the faut for the in-land crustal earthquake. Even the homogeneous medium was assumed for many previous studies, the fault rupture is supposed to penetrate to the shallow part of low velocity layer in case for breaking surface fault. This suggests that the understandings of fault behavior with consideration of low velocity layer is important. Thus, we try to investigate the fault behavior based on the model with low velocity layer and the parameter studies with changing location of asperity as the target of 2014 Northern Nagano Earthquake (Mw 6.2) with breaking surface fault.
At first, we have constructed the model with two (deep- and shallow-) asperities based on homogeneous medium that could reproduce the features of observations, such as earthquake size (seismic moment), spatial distribution of surface displacement, and the near-field ground motions (velocity and displacement time histories) with the adjustments for the stress parameters and frictional parameter (Dc). Based on this model, we have conducted the parameter studies with changing some parameters, such as stress drop, Dc, and location of asperity. The results revealed that the surface displacement is more influenced by the deep asperity than that by the shallow asperity.
The model with the shallow low velocity layer produced the area with large asperity close to the surface and showed more area of the fault surface. On the other hand, the reduction of shear modulus on the shallow part generated little difference in terms of the seismic moment. The amplitudes of the simulated near-field ground motions were amplified by the difference of impedance ratio and their shape showed more complex including reflected waves generated on the boundary of velocity layer.

Keywords: The 2014 Northern Nagano Earthquake, Dynamic Model, Asperity, Velocity Layer Structure Model

Fault Rupture Termination of the 2016 Kumamoto earthquake within Aso Caldera: Insights from Multi-Beam Back-Projection and Strong Motion Records

*Nelson Pulido[1]

1. National Research Institute for Earth Science and Disaster Resilience

In a previous study (SSJ 2024), I used the multi-beam seismic back-projection method and a dense array of near-source strong motion records from the K-NET/KiK-net networks to estimate the broadband frequency (0.1–10 Hz) fault rupture process of the 16 April 2016 Kumamoto earthquake (M7.1). In this study, I focus on the rupture termination process of the earthquake within the Aso caldera, applying the same methodology while extending the imaging target domain to encompass the caldera.
I selected 104 stations within 100 km of the hypocenter and grouped them into multiple subarrays, evenly distributed in angular regions around the hypocenter. For the back-projection target area, I constructed a 3D grid mesh with a 500 m spacing, covering a volume of 50 ×26 ×20 km from the Hinagu fault to the Aso caldera. Using the 3D S-wave velocity model of the Kyushu region (Matsubara et al., 2022), I calculated travel times for each grid-station pair. Beam power for each grid and subarray was obtained by stacking the normalized velocity envelopes at the arrival times, incorporating both source and travel times. Grid energy was evaluated at 0.25 s intervals across the 3D mesh by averaging the envelope amplitude within a ±1 s window around the arrival times. Maximum grid energies were determined as the product of the combined subarray beam energies. I investigated the source process of the Kumamoto earthquake across four frequency bands (0.1–0.5, 0.5–1, 1–5, and 5–10 Hz). My results indicate that rupture lasted for a total of 22s, propagating 45 km from the Hinagu fault to the northeastern region of Aso caldera.

High frequency ground motion radiation

High-frequency (HF) ground motions (1–10 Hz) were strongly radiated from 3 to 10 s across a broad region within the hanging wall wedge of the Hinagu fault, spanning depths of approximately 15 km to the surface. Intermediate-frequency radiation (0.5–1 Hz) was concentrated above the southern edge of the Futagawa fault at a depth of ˜5 km from 6 to 9 s (Fig. 1). The strong HF ground motion radiation estimated in this study largely overlaps with areas where JMA intensity 6 or higher were observed during the Kumamoto earthquake. This suggests that HF radiation may have been a key factor contributing to the intense shaking and widespread building damage in Kumamoto City. Additionally, the location of strong HF radiation indicates the possibility that off-fault radiation played a significant role in generating high-frequency ground motions.

Low frequency ground motion radiation

Strong low-frequency (LF) radiation (0.1–0.5 Hz) occurred north of the HF radiation zone at depths shallower than 5 km between 11 and 22 s (Fig. 1). From 11 to 16 s, LF radiation was primarily concentrated along the Idenokuchi fault, a normal fault subparallel to the Futagawa fault, where approximately 10 km of surface rupture was identified in field surveys (Fig. 1). A strong motion record of the Kumamoto earthquake observed at Nishihara Mura Komori (JMA), showed a prominent velocity pulse at about 0.2 Hz. This record was observed in close proximity to the Futagawa main fault trace and is therefore likely to reflect the shallow strong low-frequency radiation region identified in this study.

Fault rupture termination and the Aso caldera underground structure

Two distinct episodes of strong LF radiation occurred within the Aso caldera between 17 and 22 s. The first episode (17–18 s) originated beneath Nakadake volcano at depths of 1–3 km (Fig. 1), coinciding with the shallow magma chamber of the volcano, located ~1 km beneath the post-caldera central cone, as identified by ambient noise tomography of the Aso caldera (Huang et al., EPS, 2018). The second episode (18–22 s) occurred at depths of 4 km to the surface, closely aligning with the location of the Miyaji faults northeast of the Aso caldera, where surface ruptures were observed (Fig. 1). This episode likely reflects the stopping phases of the earthquake.
The location of these strong LF radiation episodes suggests that fault rupture propagated through the Aso caldera and terminated at the Miyaji faults northeast of the caldera (Fig. 1). This rupture may be linked to the extension of the Okayama-Kumamoto Tectonic Line (OKTL) through the caldera, as indicated by strong seismic reflectors aligned with the OKTL, identified in a 3D seismic reflection survey across the central cones of Aso volcano (Tsutsui et al., JVGR, 2004).

Keywords: 2016 Kumamoto earthquake, Source rupture process, Aso caldera, Broadband strong motion

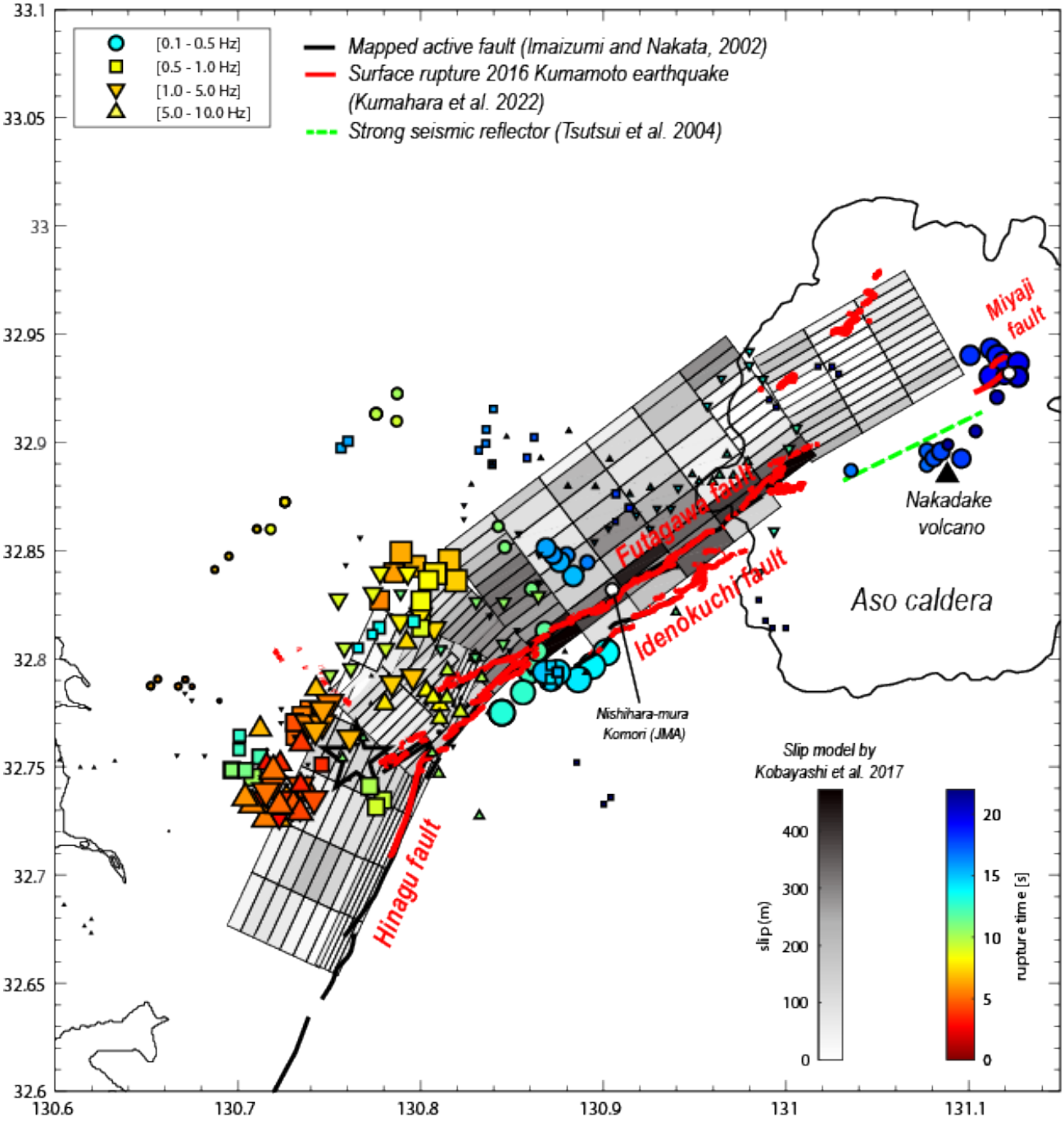

Figure 1. Broad-band frequency ground motion radiation during the 2016/04/16 Kumamoto earthquake.

Dynamic Rupture Inversion of Finite-fault with Curved Grid Finite-Difference Method: Synthetic Test and Applications

*Yuchen Zhang[1], Zhenguo Zhang[1], Zhongqiu He[1]

1. Department of Earth and Space Sciences, Southern University of Science and Technology, Shenzhen 518055, China

Dynamic source inversion can provide essential physical parameters of the fault, which enhances the resolution of seismic wave simulations and aids in risk analysis for engineering seismology, earthquake disaster loss assessment, and earthquake forecasting. However, such a task remains challenging due to its high computational demands, and when the fault geometry in the inversion differs significantly from the actual situation, the uncertain model prediction errors will exacerbate this burden and impact. We propose a novel Bayesian dynamic inversion method to infer stress and frictional parameters on faults. In the inversion, we utilize the GPU-accelerated curved grid finite difference method (CG-FDM) and an improved parallel-MCMC method to derive the model's posterior probability density function. We conduct synthetic inversion tests using the TPV8 and TPV10 models from the SCEC/USGS Spontaneous Rupture Code Verification Project. The results demonstrate that our inversion method converges to stable solutions with acceptable margins of error for both vertical strike-slip faults and moderately inclined normal faults. Subsequently, we applied this method to real earthquake events by constructing a non-planar fault model and incorporating the *b*-value distribution as a Bayesian prior constraint. Using this approach, we inverted the spatial distribution of fault friction coefficients and initial shear stress for the 2017 Mw 6.5 Jiuzhaigou earthquake, ultimately developing a three-dimensional dynamic rupture model.

Keywords: Earthquake Source Dynamic Inversion, Curved Grid Finite-Difference Method, Finite Fault Model, Parallel MCMC Algorithm

Analytical approaches for simultaneous inversion of distributed slip, Green's function, and fault geometry

*Daisuke Sato[1], Yuji Yagi[2], Ryo Okuwaki[2], Yukitoshi Fukahata[3]

1. Japan Agency for Marine-Earth Science and Technology, 2. Tsukuba University, 3. Disaster Prevention Research Institute, Kyoto University

Slip inversion is an inverse analysis of the dislocation problem that describes the motion of a medium subject to the displacement discontinuity boundary condition on faults. The current de facto standard is to calculate fault slip by assuming the shape of the fault and the solution (Green's function) of the displacement response to unit fault slip (Yabuki & Matsu'ura, 1992; Ide, 2007), but it is plagued by a solution bias derived from model assumptions (Dutta et al., 2021), which becomes an obstacle for the secondary use of estimates (Agata et al., 2021). Such model biases in slip inversions can be expressed in a unified form as an error of the integral kernel in the observation equation (Green's function of the inverse problem) (Yagi & Fukahata, 2011). Yagi & Fukahata (2011) recognized that Green's function is also an unknown unless the true model is a known, revealing that the error propagation from Green's function uncertainty can be a dominant error factor in estimating slip. Agata et al. (2021) then argue a simultaneous inversion of slip and the Green's function.

However, it should be noticed that the error in Green's function in the inverse dislocation problem is not equal to the error in Green's function in the forward dislocation problem, i.e., the fundamental solution that expresses the medium response to the source force (Hori et al., 2021), due to the presence of the error in assumed fault geometry (Matsu'ura, 1977). In conventional inversion analysis, the fault geometry works as a hyperparameter that prescribes the model to relate slip and data (Fukahata & Wright, 2008), and three-dimensional geometry estimation suffers from accuracy insufficiency (e.g., Jolivet et al., 2014). On this issue, Shimizu et al. (2021) showed that the inversion (Kikuchi & Kanamori, 1991) of inelastic strain, termed potency, can be a breakthrough that replaces the use of slip, the orientation of which is prescribed by the assumed fault shape: they clarified that the fault shape estimate as a potency-consistent boundary has the same level of accuracy as the potency estimate. However, the fault shape in Shimizu et al. (2021) is expressed by B-spline functions, so a technical difficulty remains in solving methods as B-spline expresses only a quasi-two-dimensional shape in which the dip/strike angle changes in a uniaxial direction.

We report on a formulation for simultaneously estimating the three-dimensional shape and slip of a fault plane and associate analytical expressions of the solutions. We also report that analytic representations for Green's function estimate within our formulation following Shimizu et al. (2021), where Green's function uncertainty in the inverse problem separates into Green's function uncertainty in the sense of the forward problem (the medium response uncertainty) and geometrical uncertainty of faults. This poster thus presents a method for simultaneously estimating the slip, Green's function as medium responses, and fault geometry, with analytical solutions.

In our problem setting, the model parameters are the potencies and normal and slip vectors at each coordinate on the fault plane, as well as Green's function of the observation equation. The distribution of observed data is expressed as a Gaussian distribution, and the following prior distributions are set for those model parameters: an arbitrary Gaussian distribution for the prior of the potencies, a Gaussian distribution that peaks at the reference Green's function for the prior distribution of the Green's function,

and for the normal and slip directions at each coordinate, the von Mises distribution such that the fault plane is determined as the macroscopic crack face that best explains the double-couple component of shear inelastic strain (the opening component for mode I); as a smooth surface consistent with linear continuum mechanics (Romanet et al., 2024), the crack face is then calculated. In the above problem setting, the posterior distributions of the slip, Green's function, and fault geometry are evaluated, and the optimal solution with the maximum posterior and the associated posterior covariances are calculated from the fault normals. In an advanced approach, the covariance matrix traces (variance scale factors) for the data distribution and the prior distributions of slip and Green's function are simultaneously estimated as hyperparameters, as in Yagi & Fukahata (2011).

In our poster, we will report on the verification of this formulation using synthetic tests, as well as on its application to the geodetic slip deficit inversion for the Nankai subduction zone and the teleseismic slip inversion for the 2013 Balochistan earthquake.

Keywords: Simultaneous inversion of distributed slip, Green's function, and fault geometry

Deconvolution Approach to Estimate Radiation Process of Large (Mw7.0-9.0) Earthquakes

*Keisuke Yoshida[1]

1. Tohoku University

When large earthquakes (Mw>7.0) occur, researchers immediately begin estimating their rupture processes and slip distributions. While slip distributions can be relatively easily inferred from the spatial pattern of raw geodetic data, interpreting raw seismic data is not straightforward, particularly when multiple reflected phases overlap and Green's functions become complex. Different researchers and analysis methods sometimes yield different results.

This study presents an approach using Green's function deconvolution to readily identify rupture patterns of large earthquakes (Mw6.9-9.0). This approach enables straightforward interpretation of data constraints through differences in apparent moment rate functions (AMRFs) at each station, and has been systematically applied to Mw3.0-7.0 earthquakes by Yoshida & Kanamori (2023) by using empirical Green's functions (eGF). The obtained AMRFs have also been used as waveform inversion data in several studies (Ross et al., 2017; 2018; Yoshida et al., 2020 JGR, 2022 JGR, 2023 JGR, 2023 GRL; Yoshida, 2023 JGR). While this method has been previously applied to regional earthquakes, we now utilize teleseismic data to analyze larger events.

We analyzed 27 earthquakes (Mw6.9-9.0), including 19 Japanese and 8 foreign events. BHZ channel waveforms from the GNS network were obtained through IRIS. We first determined WCMT solutions for each event using WCMT inversion by Duputel et al. (2012), then calculated synthetic waveforms for stations with available data based on these solutions. Apparent Moment Rate Functions (AMRFs) were estimated by deconvolving observed waveforms with synthetic ones. The results showed coherent azimuth-dependent variations for many events. The results showed coherent azimuth-dependent variations for many events, enabling interpretation of their physical meaning.

For example, for the 2024 Noto Peninsula earthquake, the AMRFs reveal that the rupture remained relatively quiet for the first 15 s, followed by a moderate rupture lasting about 10 s, and then two large-amplitude rupture episodes. The azimuthal dependence suggests that the second of the two episodes propagated eastward. These characteristics were consistently observed in both synthetic and empirical Green's function analyses.
In our talk, we will discuss individual results, their characteristics, and features among different earthquakes.

Keywords: Rupture process, Large earthquakes, 2024 Noto Peninsula earthquake, Moment-rate function

Analysis of Source Characteristics of Earthquakes Potentially Induced by Wastewater Injection in Peace River, Alberta, Canada

Koki Kamata[1], *Ahyi KIM[1], Jeffrey Gu[2], Wenhan Sun[2], Tai-Chieh Yu[2]

1. Yokohama City University, 2. University of Alberta

The Peace River in Alberta, Canada, is actively engaged in oil sands development. During bitumen extraction, a mixture of bitumen and water is produced, necessitating underground wastewater injection for disposal. Near these injection wells, seismic activity has been observed in swarms, and on November 30, 2022, the largest earthquake ever recorded in Alberta's history, Mw5.2 (ML5.6), occurred. This earthquake is considered highly likely to be induced (Schultz et al., 2023), and wastewater injection has continued since then, with seismic activity remaining high.
In this study, we analyze the seismic activity in the Peace River, estimate stress drop values, and investigate the relationship between injection volume and injection rate to examine differences and similarities between induced and natural earthquakes. After the November 30, 2022, earthquake, the University of Alberta installed ten seismic stations near active injection wells. This study uses seismic data recorded by these stations at a sampling rate of 250 Hz, covering 2,214 earthquakes with magnitudes ranging from -1.97 to 5.04, occurring between December 6, 2022, and April 13, 2023. However, due to operational constraints, there were two periods during which no seismic data were recorded.
Near the three active injection wells, there are a pre-existing fault and the fault responsible for the Mw5.2 earthquake, with many earthquakes occurring along these two faults, forming major seismic clusters (Sun et al., 2023). For analysis, we selected 16 events with magnitudes of 2.5 or greater and estimated their source parameters using the Empirical Green’ s Function (eGF) method. Smaller events, typically about one magnitude unit lower, were used as eGFs. The eGF method is an effective technique for accurately extracting source parameters by assuming that a small earthquake occurs in the immediate vicinity of a larger event, thereby eliminating the effects of path propagation and instrument response to isolate the source characteristics. In this study, we applied a bandpass filter of 0.5–2.0 Hz to the waveforms, calculated their correlation, and selected the three events with the highest average correlation values as eGFs.
The analysis results showed that the estimated stress drop values ranged from approximately 1 to 10 MPa, which is comparable to those of tectonic earthquakes. This suggests that the earthquakes analyzed in this study were likely triggered by stress perturbations caused by the Mw5.2 earthquake. However, as wastewater injection has continued, the spatial expansion of seismicity has been observed. Additionally, seismic activity increased significantly after March 2022, when injection volumes sharply increased, suggesting that wastewater injection also contributes to ongoing seismic activity. In the future, we plan to analyze smaller earthquakes and data from other seismic networks recorded before December 6, 2022, to further investigate detailed source characteristics and examine the relationship between wastewater injection and induced seismicity in greater detail.

Keywords: wastewater injection, induced earthquake, stress drop, source characteristics

Reproduction of interplate slip phenomena along the Nankai Trough: Deep short-term slow slip events

*Fuyuki Hirose[1]

1. Seismology and Tsunami Research Department, Meteorological Research Institute

Introduction

Various types of slip phenomena occur between plates along the Nankai Trough, including great earthquakes and slow earthquakes, depending on the depth [e.g., Obara & Kato 2016, Science]. In particular, short-term slow slip evens (SSSEs) and deep tremors are distributed in a belt-like zone with several segmentations [e.g., Obara+ 2010, GRL; Okada+ 2022, EPS].

To elucidate the slip phenomena between plates, simulation studies based on the rate- and state-dependent friction (RSF) law have been conducted [e.g., Matsuzawa+ 2013, GRL; Hirose+ 2022, EPS]. Matsuzawa+ [2013] reproduced deep tremors, SSSEs, and LSSEs in the Shikoku region using the RSF law that introduced a cutoff velocity (cutoff time) that represents the characteristics of laboratory experiments using halite [Shimamoto 1986, Science]. In this case, SSSEs were expressed by continuous rupture of tremor patches.

Targeted phenomena

In this study, our targeted phenomena are deep SSSEs along the Nankai Trough. The Mw is about 5.5 to 6, the duration is about 4 days, and the recurrence interval is about 3 to 12 months [e.g., Nishimura+ 2013, JGR]. Slow earthquakes also move along the strike direction at a speed of about 10 km/day [Obara+ 2012, GRL]. The activity and slip amount of SSSEs are large in Ise Bay, eastern Shikoku, and western Shikoku [Okada+ 2022].
The areas where SSSEs and tremors occur largely overlap, but the activity of tremors is low in Ise Bay [Obara+ 2010]. With the same settings as in the previous study [Matsuzawa+ 2013], which expressed SSSEs by continuous rupture of tremor patches, it is not possible to generate SSSEs in areas without tremors. Therefore, we did not place tremor patches and simply gave various parameters as functions of depth.

Model

We modeled the 3-D plate interface from the Tokai region to the Hyuga-Nada Sea, and 53,550 triangular cells with sides of ~2.5 km are arranged. The plate convergence rate is 1.0 cm/y at the eastern end and 5.5 cm/y at the western end [Nishimura+ 2018, Geosphere].

In this study, we adopted the RSF law that introduces a cutoff time with a cutoff time t_{cx} into the aging law [Yoshida+ 2013, JGR]. The friction parameter a is constant at 0.005 for all cells. The friction parameters a-b are set to -0.003 at depths shallower than 35 km and +0.003 at depths deeper than that. The effective normal stress σ, characteristic distance L, and cutoff time t_{cx} are changed in five depth ranges: 1) depths shallower than 10 km, 2) 10–20 km, 3) 20–30 km, 4) 30–35 km, and 5) deeper than 35 km.

Results

In our simulation, Mw 8-class earthquakes occurred at depths shallower than 20 km, LSSEs occurred at depths of 20–30 km, and SSSEs occurred at depths of 30–35 km. The SSSEs were larger in scale in Ise Bay and western Shikoku, which is consistent with the observations. In these regions, the plate boundary is

shallower than in the surrounding areas and has width in the dip direction, so it is thought that the SSSEs become larger in scale due to stronger locking after one slip. However, it should be noted that the SSSEs are low in eastern Shikoku and active in the Kii Channel, which is different from the observations. The SSSEs occur at intervals of about 3 months to 1 year, and the slip migration speed is about 10 km/day, which is consistent with the observations. In some cases, SSSEs are excited by the influence of LSSEs on the updip side, shortening the interval between SSSEs.

Keywords: Nankai Trough, Short-term slow slip events, Simulation, Cut-off time

Relationship between the Boso slow slip events and the accompanying earthquake swarm: Part 2

*Issei Yasuhara[1], Toshinori Sato[2]

1. Graduate School of Science and Engineering, Chiba University, 2. Graduate School of Science, Chiba University

1.Introduction
Slow slip events (SSEs) are phenomena that, unlike normal earthquakes, slowly slide across plate boundaries without radiating seismic waves. SSEs are detected by continuous observation of crustal deformation using geodetic techniques, and their occurrence has been reported in Japan and around the world. Further understanding of SSEs is considered necessary to reveal the mechanisms of stress accumulation and release at plate boundaries, as well as to clarify important issues in seismology, such as the prediction of large earthquakes.
In the off Boso area, short-term SSEs with a duration of several to several tens of days have occurred seven times from 1996 to 2024 with intervals of about 2 to 7 years. The Boso SSEs involve earthquake swarms.
The occurrence of the SSEs and the swarm activities are thought to be related: in the 2007 and 2011 Boso SSEs, the slip of the SSEs and swarm activities were well correlated in time and space, suggesting that the SSEs may have induced the swarm activities (Hirose et al, GRL, 2014). Yasuhara and Sato (JpGU, 2024; Seismological Society of Japan, 2024) obtained ΔCFF for the 2002 and 2007 swarms occurred with the SSEs, suggesting the possibility of fluid movement.
In this study, we examine whether the 2011, 2014, and 2018 Boso SSEs induced the associated swarms and consider the factors that cause the swarms.

2.Analysis method
An ABIC inversion analysis was performed on daily coordinate values (F5 solution) of GNSS data by GSI GEONET to estimate the spatio-temporal distribution of slip of the SSEs. From the obtained slip distribution, we calculated ΔCFFs due to the SSEs on the faults of the swarms. ΔCFFs were calculated for the swarms of Mw 3.5 or greater (5 in 2011, 4 in 2014, and 13 in 2018) that occurred during and one month after the SSEs. We used focal mechanism solutions by the F-net of NIED.

3.Results
Of the ΔCFFs obtained, 40 % (2/5 faults) in 2011, 50 % (2/4 faults) in 2014, and 38 % (5/13 faults) in 2018 were above 0.01 MPa, a condition empirically considered earthquake-prone. These results indicate that the SSEs that occurred in 2011, 2014, and 2018, did not directly trigger the swarms. Therefore, we considered the change in pore pressure that would cause ΔCFF to be above a threshold value of 0.01 MPa for the faults of the swarms.
The change in pore pressure was estimated about 0.05~0.18 MPa increase for the faults of swarms that occurred near SSE’s slip area during the SSEs. Kobayashi and Sato (GRL, 2021) estimated effective normal stress (10~50 MPa) in the area of the Boso SSEs, which is very small compared to lithostatic stress (350~600 MPa), suggesting the presence of high pore pressure. The same analyses as in this study for the 2002 and 2007 SSEs also estimated an increase in pore pressure of about 0.03~0.2 MPa. These results suggest that the slips of the SSEs may have caused fluid migration from its slip area to the fault of the swarms.
Therefore, it is considered that the swarms were triggered by the SSEs through an indirect factor of fluid movement from the slip region of SSEs to the faults of the swarms.

Acknowledgements
Daily coordinates of GSI GEONET (F5 solution) were used. Coulomb 3.4 from the U.S. Geological Survey was used to calculate stresses. Data from F-net of NIED were used for the mechanism solution of earthquake swarms. This research was supported by Grant-in-Aid for Scientific Research (23K03541).

Keywords: slow slip, earthquake swarm, ΔCFF, fluid movement

High-resolution estimation of the Boso Slow Slip Events in 2011, 2013–2014, 2018, and 2024 based on inflection point analysis of high-rate GNSS data

*Yuta Mitsui[1], Riko Arai[1], Shiori Watanabe[1,2]

1. Shizuoka Univ., 2. Univ. of Tsukuba (currently)

Previous research by Fukuda (2018) utilized daily solutions of Global Navigation Satellite System (GNSS) data from 1996 to 2014 to conduct an inversion analysis based on the network inversion filter. The study demonstrated that the nucleation patterns of slow slip events (SSEs) off the Boso Peninsula were not uniform. For example, the nucleation of the 2011 SSE was more rapid, whereas the 2013–2014 SSE initiated more gradually.

This study focuses on the diversity of SSEs. We estimate the detailed spatiotemporal evolution of four Boso SSEs—those occurring in 2011, 2013–2014, 2018, and 2024—using precise point positioning (PPP) solutions sampled at five-minute intervals from high-rate GNSS data provided by the Nevada Geodetic Laboratory. To fully utilize the high temporal resolution of GNSS, we apply change-point detection based on sparse modeling, as proposed by Taylor & Letham (2017), to extract key characteristics related to the onset, growth, and termination of each SSE from the time-series data at individual observation sites. Subsequently, we employ a Hamiltonian Monte Carlo method incorporating a horseshoe prior distribution (Carvalho et al., 2009) to estimate the spatiotemporal evolution of slip distribution, allowing for localized regions of significant slip. Although the temporal resolution varies slightly among events, we set it to approximately 20 hours, which is less than one day.

As a result, we successfully characterized the four SSEs. The 2011 SSE occurred "at the most inland location," "propagated relatively simply in the up-dip direction," and exhibited "a more abrupt onset than termination." The 2013–2014 SSE occurred "offshore, distinct from the 2011 SSE," and was "smaller in scale with limited propagation." The 2018 SSE "initiated at a location similar to the 2013–2014 SSE, with slip extending partially into the 2011 SSE region," "propagated offshore with a change in direction toward the end," and had "a termination more abrupt than its onset." The 2024 SSE "occurred in a similar location to the 2013–2014 SSE but was larger in scale."

Although SSEs are broadly categorized as "repeating events," our findings suggest significant variability among individual occurrences. Unlike earthquakes, SSEs are expected to have minimal effects from dynamic rupture processes, implying that quasi-static frictional heterogeneity on spatial scales of less than approximately 10 km may play a crucial role.

Keywords: SSE, Boso Peninsula, Slip distribution, Inflection point analysis

Mapping Fault Zone Attenuation Using MiDAS Downhole Optical Fiber and Borehole Seismic Arrays

*Lu Hsiao[1], Kuo-Fong Ma[1,2], Yen-Yu Lin[1]

1. Institute of Geophysics, National Central University, 2. Institute of Earth Sciences, Academia Sinica

Fault zone architecture offers critical insights into earthquake dynamics. The structural components of a fault zone, including the fault core, damage zones, and surrounding host rocks, play pivotal roles in seismic behavior. The quality factor (Q), representing seismic attenuation (Q^{-1}), is inversely related to the degree of fracturing within these zones; higher fracture densities typically correspond to lower Q values, indicating greater energy dissipation. Moreover, the permeability of these fractured zones facilitates fluid migration, which can alter fault strength and affect earthquake nucleation processes. The Milun Fault, an active east-dipping, left-lateral reverse fault, is located in the northern section of Taiwan’ s Longitudinal Valley, near the boundary between the Eurasian Plate and the Philippine Sea Plate. This fault has been responsible for multiple major earthquakes, including the 1951 Longitudinal Valley Fault Earthquake and the 2018 Hualien Earthquake. The Milun Fault Drilling and All-inclusive Sensing Project (MiDAS) initiated a scientific drilling with two boreholes operation in 2021 integrated with optical fiber sensing and borehole seismometers in 2022. The MiDAS Hole-A intersects the recent slipped fault zone at 520-540m providing the unique opportunity to map fault zone attenuation architecture using high spatial resolution of distributed acoustic sensing (DAS) and borehole seismometer arrays. To characterize the detail attenuation structure, we estimate the attenuation factor Q along MiDAS Hole-A using DAS records, with borehole seismometer data for validation. Our analysis focuses on seismic events approximately 20 km from the borehole site between June and December 2023. Before exploring the high-resolution attenuation mapping within the fault zone using DAS (4m spatial resolution), we first examine two depth station pairs: borehole seismometers MDSA1 and MDSA5 (positioned at 94 m and 638 m, respectively) and optical fiber nodes 1257 and 1390 at corresponding depths. The datasets are in acceleration and strain-rate, which are subsequently integrated into velocity and strain, respectively. We applied the STA/LTA method to identify the seismic arrivals and use polarization analysis to select events with incidence angles below 45°. Arrival time and effective shaking duration (ESD) are used to define P-, S-wave, and noise windows for frequency-domain analysis. We compute the spectral ratios between stations to estimate the attenuation parameters, Q_p and Q_s, from Δt_p^* and Δt_s^* by applying least-squares fitting. Preliminary results indicate consistently low Q (with 10s of values) across the fault zone, with comparable estimates from DAS and borehole seismometers at depths of 94 m to 639 m. Further analysis will refine the attenuation character within fault zone and explore the potential of fiber-optic data for achieving high-resolution attenuation mapping along the fault zone.

Keywords: Milun Fault, Seismic attenuation, Fault-zone attenuation, Milun Fault Drilling and All-inclusive Sensing Project (MiDAS), Distributed Acoustic Sensing (DAS)

Calcite-bearing cataclasite and non-double-couple earthquakes in the aftershock area of the 2000 Tottori-ken Seibu earthquake

*Kiyokazu Oohashi[1], Kenta Kobayashi[2]

1. National Institute of Advanced Industrial Science and Technology , 2. Department of Geology, Faculty of Science, Niigata University

Generally, fault ruptures occur as shear that moves parallel to the fracture (mode II or mode III fractures), and the equivalent force couple for fault motion is a double couple, represented as slip along a single planar fault. However, non-double-couple(NDC) earthquakes, which cannot be explained by double couple mechanisms, have also been reported in volcanic regions and geothermal areas, suggesting the complexity of fault geometry and rupture processes and/or presence of fluids. Hayashida et al. (2020, GRL) reported NDC earthquakes with magnitudes of 1 to 3 in the aftershock area of the 2000 Tottori-ken Seibu earthquake, observed through hyper-dense seismic monitoring, and suggested that many of these could be explained by tensile-shear rupture mechanisms.
In this study, we analyze calcite-bearing fault rocks from the aftershock area of the 2000 Tottori-ken Seibu earthquake using geological methods to elucidate the relationship with NDC earthquakes. The fault rocks were collected from an outcrop on the western side of Ryokusuiko Lake in Nanbu-cho, Saihaku-gun, Tottori Prefecture (Aizawa et al., 2005, JGSJ; Suzuki et al., 2016, JpGU). The fault rocks consist of a consolidated zone (cataclasite zone) and an unconsolidated, continuous slip zone (fault gouge zone). Based on polished section and thin section observations, the fault rocks are divided into seven components (in order of formation): I. Ultracataclasite zone, II. Weakly foliated cataclasite zone, III. Phyllosilicates-bearing cataclasite zone (fragmented), IV. Fault-parallel calcite veins, V. Illite-bearing fault gouge, VI. Fault-perpendicular calcite veins, VII. Smectite-bearing thin gouge zone. I, IV, and VII exhibit structures indicative of seismic rupture or slip(implosion breccia and principal slip zone). The calcite associated with II, IV, and VI presents a coarse granular, polygonal texture without fibrous or elongation crystal structures. Since the host rock, granite, does not contain calcite, it is inferred that the calcite precipitated rapidly from fluids on fault planes opened during seismic events. The cumulative fault displacement is estimated to be ≧5.4 m from the offset of host rock, and number of deformation events are estimated to be seven from microstructural observations. Assuming a constant displacement per event, the lateral displacement per event is ≧0.77 m. The opening displacements for II and IV are up to 5 mm, yielding an opening to lateral displacement ratio of ≦0.006. This value consistent with the tensile angle reported by Hayashida et al. (2020, GRL) (approximately 0.2 to 6 degree, equivalent to an opening to lateral displacement ratio of about 0.003 to 0.1). Thus, the formation of calcite veins on fault planes could explain the occurrence of NDC earthquakes observed in this region.

Keywords: fault rock, tensile shear, geofluids, mineral vein

Seismic Fault Repetition Estimated from Pseudotachylyte in Eidsfjord, Northern Norway

*Asuka Tsuda[1], Takamoto Okudaira[1]

1. Osaka Metropolitan University

Introduction: Pseudotachylytes, are fault rocks that record seismogenic fracturing and deformation structures, and thus their formation processes provide crucial insights into earthquake generation processes. Since pseudotachylyte is likely to have overlapped different late-stage events, such as retrograde metamorphism and brittle and/or plastic deformation, a comprehensive understanding of the formation and development process requires careful observation of the fracturing and deformation structure. In the Eidsfjord region of Northern Norway, the lower crust is widely exposed, and pseudotachylytes associated with crustal-scale detachment faults have been identified (e.g., Markl, 1998). This study aims to clarify the microstructural and chemical characteristics of minerals in anorthosites containing multiple pseudotachylyte injection veins, elucidate their formation process and consider the deformation processes in the seismogenic regions based on estimating the formation temperature conditions of the pseudotachylyte veins.
Methods: The details of microstructures in the deformed anorthosites were observed using a polarization microscope and a scanning electron microscope (SEM). Mineral chemical composition analysis was conducted using an energy-dispersive X-ray spectrometer (EDS). The formation temperature of the pseudotachylyte veins was estimated mainly using pyroxene chemistry based on pyroxene thermometer (Lindsley, 1983). Furthermore, the phase equilibrium calculation program MELTS was used to model the melting process associated with pseudotachylyte formation.
Results: The constituent minerals of the host anorthosite include plagioclase, orthopyroxene, clinopyroxene, orthoclase, quartz, biotite, magnetite, ilmenite, and rutile. In the pseudotachylyte, plagioclase, clinopyroxene, orthoclase, and magnetite which are considered to be crystallized from the melt are observed. Three types of pseudotachylyte (Pt-1, Pt-2, Pt-3) with significantly different mineral sizes and morphologies, as well as a fine-grained zone with notable fracturing, are identified. No significant differences were found in the chemical composition of the matrix portions of the three types of pseudotachylyte. Pt-1, which exhibits a decussate texture indicative of rapid crystal growth, cuts through the fine-grained zone, while Pt-2 truncates both. Additionally, Pt-1, Pt-2, and the fine-grained zone are displaced along the same fracture, while Pt-3 is found along fractures or near the boundary between Pt-2 and the host rock. The pyroxene thermometer results show that the crystallization temperatures of pyroxene in the host rock and pseudotachylyte are ~600 ˚C and ~1000 ˚C, respectively.
Discussion: The presence of three different pseudotachylytes in the anorthosite sample, which differ significantly in mineral size and morphology, and their structural features, which show a clear order of formation, suggest that at least three melt injections have occurred. However, the lack of significant differences in the chemical composition of the matrix portions of the pseudotachylyte implies that fracturing and melting repeatedly occurred within the brittle regime of the shear zone. The crystallization temperature of pyroxene in the pseudotachylytes (~1000 ˚C) represents the temperature at which pyroxene crystallized from the pseudotachylyte melt, meaning that the melt formation temperature must have been higher. Using MELTS, the energy required to melt the host rock was estimated to be at least 27.14 MJ/m^3. We will discuss earthquake magnitude and other factors based on the estimated melting energy.

References: Markl G (1998) NGU-Bull 434, 53-75; Lindsley DH (1983) American Mineralogist 68,

477-493.

Evaluation of fluidization during earthquake slip at the primary slip zone in the Neogene accretionary complex, Boso Peninsula, Japan

*Tatsuru Fukuta[1], Tetsuro Hirono[1]

1. Osaka Metropolitan Univercity

Dynamic fault weakening during earthquake slip on a fault affects the slip behavior. For example, at the 1999 Chi-Chi earthquake in Taiwan and the 2011 Tohoku-Oki earthquake, thermal pressurization (TP) was considered to occur on their faults, which could enhance the rupture propagation and could resultantly increase the amount of fault slip. In the case that the rupture reaches the trench, a large uplift of the seafloor might trigger huge tsunami. Therefore, it is significantly important to elucidate the dynamic weakening mechanism on their faults. In this study, we focus on the primary slip zone (PSZ) in the Neogene Hota Group, the Boso Peninsula in which TP is considered to function on the fault on the basis of its geochemical analyses and modellings. we performed the field investigation, collection of the fault samples, microscopic observation, and spatial analysis of major elements by using an electron probe micro-analyzer. In the PSZ, grain-size reduction and developments of layered and/or flow structures are characteristics by comparing with each surrounding rocks. Because the flow structure may form during fluidization related to earthquake events, we performed the numerical analysis to determine the fundamental parameter of fluid dynamics such as the Reynolds number, and estimated the viscosity to be 1.68×10^{-3}. This could indicate that turbulent flow occurred in the PSZ during earthquake slip. In addition, the fluidization in the slip zone may enhanced pore-fluid pressure that may assist the function of TP.

Quantitative evaluation of surface fracture energy in minor fault adjacent to the Taiwan Chelungpu fault

*Takumi Kawakami[1], Tetsuro Hirono[1]

1. Osaka Metropolitan University

The earthquake drives the release of stored elastic strain energy accumulated on the fault, which is distributed as dissipated energy and radiated energy. The energy budget is essential to estimate the earthquake's scale and the fault's stress level. However, the energetics of minor faults, which is here defined as a fault has roughly a small thickness less than 1cm and/or a slip distance under 1 m, rarely have been studied. Thus, we tried to estimate the surface fracture energy from the minor fault obtained TCDP, having 1-cm thick black gouge, by analyzing grain images under scanning electron microscope (SEM) and optical microscope.
We obtained the surface fracture energy by applying the formula of $U = A_{SZ} \gamma \lambda$ (Chester et al. , 2005), in which A_{SZ} is the surface area per meters squared area during the slip, γ is a specific fracture energy, and λ is the correction value. We obtained $A_{SZ} = 1.5 \times 10^{4}$ m^2 per meter squared area by calculating through images of microscopes for the minor fault. By assuming $\gamma = 1$ J/m^2 and $\lambda = 6.6$, we estimated that the surface fracture energy of the minor fault is 0.1 MJ/m^2. In addition, we tried to assess the breakdown work of the minor fault by using this value. Assuming the ratio calculated by Ma et al. (2006) of breakdown work to surface fracture energy, 6%, we estimated the value of 1.68 MJ/m^2. We also estimated the seismic moment of the minor fault. By assuming that the fault length is several cracks length observed on outcrops, 2–60 m and by apllying empirical formulas for Matsuda (1975) and Iio (1986), we obtained the values of the seismic moment to be 4.6×10^{9} –1.1×10^{13} Nm.
We compared these data with the scaling law which was estimated the breakdown work and the seismic moment through earthquake observations by Cocco et al. (2008), and found that the values of the minor fault is out of the law. In the presentation, we will show more updated discussion.

Keywords: surface fracture energy, breakdown work, seismic moment

Investigating Smectite Content in Neodani Fault Gouge: A Quantitative Approach to Understanding of Fault Mechanics

*Bosco de Sousa Auxilio[1], Tomoyuki Ohtani[1]

1. Gifu Univ.

The Neodani Fault, famous for its activity during the 1891 Nobi Earthquake, presents a unique opportunity to delve into the mineralogical and geochemical composition of fault gouges. The relevance of smectite in fault mechanics is underscored by its role in modulating the stability of fault zones and influencing the dynamics of seismic events. Furthermore, the spatial distribution and concentration of smectite within fault gouge can provide valuable information about the geological history and tectonic processes in a region, making it an essential focus of study in geomechanical research.
This study investigates the quantitative analysis of smectite in Neodani Fault gouge using two primary methods: the XRD RockJock method (Eberl, D.D., 2003) and the Methylene Blue Adsorption test (Miyoshi et al., 2016). Samples analyzed in this study were sourced from borehole NDFD-1-S1 drilled by the Nuclear Regulation Authority and an outcrop sample. The Methylene Blue Adsorption test is employed to measure the cation exchange capacity (CEC) of the smectite in the fault gouge. This test leverages the high adsorptive capacity of smectite for methylene blue dye, which quantitatively binds to cation exchange sites. The XRD RockJock method utilizes X-ray diffraction data analyzed through the RockJock software to quantify the mineralogical composition of the fault gouge. This method is particularly advantageous due to its accuracy and ability to handle small sample sizes, making it suitable for analyzing the often-limited quantities of fault gouge material available. Prior to analyzing these samples, both methods were calibrated using Kunigel V1 Bentonite samples with measured value range from 46% - 49 % Smectite content (Ito et. al, 1998). Calibration results indicated that RockJock program generally showed a slightly lower smectite content than the calculated value compared to the Methylene Blue Adsorption test which 2 out of 3 samples falls in the range of the calculated value, but both methods consistently indicated the presence of smectite.
The RockJock analysis revealed significant smectite presence, alongside primary minerals identified, including quartz, plagioclase, and potassium feldspar. For the outcrop sample, smectite content was determined to be 2.34% by RockJock and 3.841% by Methylene Blue test. Despite its low content, the presence of smectite suggests potential plasticity. For drilling samples from NDFD-1-S1, analyzed by XRD, fault gouge from the latest slip zone (basalt protolith) showed the highest smectite content, around 49.7%, compared to other gouges from older slip zones, which showed 32% and 35% (also basalt origin), and merely 4.38% for mudstone-derived gouge. The differing smectite content in drilling samples, even from the same lithological origin, can be attributed to differences in environmental conditions, hydrothermal alterations, and degrees of deformation.
The highest smectite content in the latest slip zone suggests that the basalt-origin fault gouge underwent extensive hydrothermal alteration and deformation, facilitating smectite formation, which may reduce shear strength and make it prone to slip. In older slip zones also of basalt origin, slightly lower smectite content (approximately 32% and 35%) implies less hydrothermal alteration or different deformation histories, potentially resulting in more frictional strength compared to the latest slip zone. In contrast, the lowest smectite content (around 4.38%) in mudstone-derived gouge indicates less alteration and plasticity, making these zones more brittle and prone to stick-slip behavior. Differences in smectite content based on lithology significantly impact fault mechanics. High smectite content in basalt-derived gouges suggests enhanced plasticity and lower shear strength. Conversely, the lower smectite content in mudstone-derived gouges may result in higher frictional strength. Understanding these variations can

help predict fault behavior and inform earthquake hazard assessments.

Keywords: Neodani, Fault-gouge, XRD-RockJock, Methylene Blue

Relationship between deformation structure and seismic slip in the shallow part of the Neodani Fault zone

*Tsuyoshi Maeda[1], Tomoyuki Ohtani[2]

1. Gifu University Graduate School of Natural Science and Technology, 2. Faculty of Engineering, Gifu University

A Shallow fault zone has not been considered an important part because they cannot accumulate large strain energy. However, during the 2011 off the Pacific coast of Tohoku Earthquake, fault slip was estimated to have increased in shallower areas, with a 65 m slip at the trench axis (Sun et al., 2017). Lin et al. (2017) also found that a comparison of stress conditions before and after the Tohoku-Pacific Ocean Earthquake showed that the shallow part of the plate boundary fault near the Japan Trench released accumulated stress and energy, which was one of the factors causing the large fault slip. This suggests that in earthquakes occurring at plate boundaries, the stress release in shallow fault zone is responsible for the increased slip. On the other hand, it is unclear whether this phenomenon occurs at the shallow fault zone in intraplate earthquakes. This should be clarified.
The Neodani Fault is rupture during the 1891 Nobi earthquake, one of the world's largest inland earthquakes. The maximum displacement in the Nobi Earthquake was 8 m in left lateral displacement and 6 m in vertical displacement (Muramatsu et al., 2002). Ohtani et al. (2024) observed core samples taken from a borehole drilling at Neomidori, and found a high possibility that the fault was weakened by thermal pressurization at a depth of 380 m. Therefore, the purpose of this study is to observe deformation structures of the Neodani Fault at depths shallower than 100 m, and to clarify the relationship between depth and phenomena occurring in and near the slip zone caused by seismic faulting.
In this study, we observed surface outcrops and borehole core samples containing the latest slip surface of the Neodani Fault. The surface outcrops and borehole locations are located in the Neonagamine, Motosu City, Gifu Prefecture, Japan. Holes R3NDFP-1 and R3NDFD-1 were drilled by the Nuclear Regulation Authority at an angle perpendicular to the strike of the Neodani Fault. Hole R3NDFP-1 was drilled toward the direction of 60˚ from the horizontal plane with a total length of 30 m and penetrates the latest slip zone at a drilling depth of 16 m. Hole R3NDFD-1 was drilled toward the direction of 82˚ from the horizontal plane with a total length of 80 m and penetrates the latest slip zone at a drilling depth of 65 m. Rock thin sections were prepared from each sample at surface outcrop, 16 m depth, and 65 m depth, and BSE images were observed by SEM.
Observations show that barite (barium sulfate) is included in all rock thin sections. Barite was only found around the latest slip zone in the surface outcrop. Barite distributed in fractures and radial barite was found at depths of 16 m and 65 m. Barite vein is recognized at depth of 65 m.
Barium sulfate is known to be almost insoluble in water, but its solubility increases with increasing temperature from 0 ˚C to 100 ˚C and decreases at temperatures higher than 100 ˚C, and its solubility increases with increasing pressure (Shi et al., 2023). This suggests that barite was formed through the following processes.
First, faulting causes thermal pressurization, which increases the temperature and pressure around the slip zone and dissolved barium sulfate into the pore water. Next, cracks caused by faulting are filled by the pore water with dissolved barium sulfate. Finally, the temperature of the pore water decreases and barium sulfate precipitates in the cracks.
Thus, barite may be evidence of increased temperature and pressure due to thermal pressurization during faulting, which may have promoted seismic slip in the shallow part of the inland fault.

References:

Ohtani et al. (2024) Proceedings of the 131st Annual Meeting of Geological Society of Japan, G5-O-2.
Muramatsu et al. (2002) The 1891 Nobi Earthquake and Neo-dani Fault Zone, Kokon Shoin, Tokyo (in Japansese)
Lin et al. (2017) Journal of Geography, 126, pp.223-246.
Sun et al. (2017) Nature Communication, 8, 14044.
Shi et al. (2023) ACS Omega, 8, pp.20440-20449.

Keywords: fault, thermal pressurization, Barite

Off-fault Damage Development as Revealed by Fault Surveys

*Kosei Ogita[1], Jun Muto[1], Hiroyuki Nagahama[1], Sando Sawa[1]

1. TOHOKU UNIVERSITY

Off-faults of large-scale strike-slip faults, such as the San Andreas fault (SAL) and the Arima-Takatsuki Tectonic Line (ATTL), are known to contain characteristic fault rocks, called “pulverized rocks” (e.g., Brune, 2001; Dor et al., 2006a; Mitchell et al., 2011; Muto et al., 2015). They are typically characterized by a lack of shear strain and a development of significant crack in minerals. These features indicate that pulverized rocks are formed by a dynamic rupture different from a general fault slip (Muto et al., 2015). On the other hand, the number of samples is still too small to fully understand this comminution process, and conditions and factors related to the formation of pulverized rocks remain unclear, such as the presence of minerals altered by hydrothermal fluids in the ATTL (Shimizu et al., 2021). In this study, we investigated fractured granites in the Off-fault of the Itoigawa-Shizuoka Tectonic Line (ISTL), where new pulverized rocks have been suggested to exist, to better understand the formation process of pulverized rocks. As a result, rocks with the same characteristics as previously reported pulverized rocks were found in the off-fault of the ISTL’ s thrust fault. In addition, we conducted a detailed and quantitative record of off-fault damage within a few meters near the fault core using the fractal dimension of the particle size distribution. The presence of the new pulverized rocks in the ISTL discovered in this study is the first example of pulverized rocks found in not only a strike-slip fault but also a thrust fault and indicates that comminution is likely to be a more universal phenomenon that is independent of fault morphology and alteration. Also, fractal dimension measurements show a wide range of high fractal dimensions close to 3 that are indicative of impact comminution. This suggests that high-energy dissipation occurs near the fault core. The damage heterogeneity recorded in the entire off-fault is also observed in the highly pulverized rocks in the vicinity of the fault. This off-fault damage heterogeneity is known to produce variations in the strain rate field and strength of the rock, which in turn affects seismic wave propagation and energy dissipation processes during the next earthquake (Ostermeijier et al., 2022). Therefore, this study provides new information on the off-fault damage of fault pulverized rocks, which is important for understanding the energy dissipation process during earthquakes, especially in the vicinity of faults.

Keywords: Pulverized Rocks, Off-fault damage, Itoigawa-Shizuoka Tectonic Line

Deformation mechanisms of quartz in plate boundary rocks deformed in a deep slow earthquake source region

*Shota Komagino[1], Kohtaro Ujiie[1], Thomas Yeo[1], Norio Shigematsu[2]

1. University of Tsukuba, 2. National Institute of Advanced Industrial Science and Technology

Block-in-matrix fabric, characterized by blocks embedded in a weaker matrix, is commonly observed in plate boundary rocks exhumed from deep slow earthquake source regions. Numerical models suggest that deep slow earthquakes arise from by heterogeneous deformation of mélange zones characterized by block-in-matrix fabric. However, the deformation mechanisms, shear strength, and strain rates during mé lange formation remain unclear. Here, we investigate the Nishikashiyama mélange, which was exhumed from a deep slow earthquake source region, comparable to the Nankai subduction zone beneath Shikoku. Viscous shear in the mélange is localized along the chlorite-actinolite schist, with a shear direction consistent with north-northwest subduction along a NE-SW striking paleo-Pacific margin. Within the chlorite-actinolite schist, quartz veins lenses are embedded in the matrix. Microstructural observations and electron backscatter diffraction analysis of these quartz lenses reveal a strong crystallographic preferred orientation and high grain orientation spread values. Quartz exhibit microstructures indicative of recrystallization, primally through subgrain rotation, with lesser contributions from grain boundary migration. Dislocation creep and dislocation-accommodated grain boundary sliding are the primary deformation mechanisms, with basal-a slip and prism-c slip as the dominant active slip systems. The shear strength and strain rate of chlorite-actinolite schist, estimated from the quartz recrystallized grain size piezometer and quartz flow law are ~50 MPa and ~5.3×10^{-10}-7.6×10^{-10} s^{-1}, respectively. In contrast, grain boundary migration mainly controlled the microstructure in quartz veins located outside the chlorite-actinolite schist. This contrast in microstructures between the inner and outer chlorite-actinolite schist suggests an increased strain rate along the chlorite-actinolite schist, which may correspond to the occurrence of slow slip events along the chlorite-actinolite schist.

Keywords: block-in-matrix fabric, quartz, dislocation creep, rheology, deep slow slip, EBSD

Shear zone development in the deep part of subduction zone recorded in the Kerama Islands, Okinawa

*Kei Takahashi[1], Asuka Yamaguchi[1], Makoto Otsubo[2]

1. The University of Tokyo, 2. National Institute of Advanced Industrial Science and Technology

Slow earthquakes, characterized by slow slips compared to regular earthquakes, have been observed along the plate boundaries in subduction zones from seismological and geodetic studies. Deep slow earthquakes, which occur at greater depths than the sources of megathrust earthquakes, are thought to occur in ductile shear zones where temperatures exceed 350˚C (Behr and Burgmann, 2021; Kirkpatrick et al., 2021). However, identifying deformation features of geological outcrops specifically attributable to slow earthquakes remains a significant challenge due to the overprinting by multiple deformations, metamorphic processes, and uplifting processes. Therefore, this research aims to find deformation processes occurring in the deeper parts of subduction zones by analyzing deformed rocks formed under pressure-temperature conditions corresponding to deep slow earthquakes with minimal retrograde deformation and metamorphism.

In this study, we focus on understanding shear zone formation and its deformation mechanisms in the Kerama Islands, Okinawa Prefecture. The research area, the Kerama Islands, are located west of Okinawa Island. They belong to the Ryukyu Arc (Takami et al., 1999) and contain high-grade metamorphic rocks (epidote-amphibolite metamorphic facies with maximum temperature of approximately 530˚C) in the Shimanto Belt (Yamamoto, 2021JpGU). Especially in Aka Island, it is reported that shear zones developed near the boundary between greenstone and sandstone exhibit highly deformed features like mylonite (Yamamoto, 2021JpGU).

We adopted several methods with different scales to investigate the types of deformed rocks and their deformation characteristics in this region, with a particular focus on the distribution and deformation mechanisms. A field survey was conducted in October 2024 to observe the overall picture of the shear zone in Aka Island. Chemical composition mapping by using micro-XRF and thin-section observation were performed to investigate microstructures of highly deformed samples.

As a result, the deformation structures and compositions of the shear zone on Aka Island were characterized across scales ranging from micrometers to approximately 100 m. The shear zone is about 160 meters wide, but the degree of deformation within the rocks is heterogeneous. Highly deformed sections (mylonites) are localized within the shear zone and the layers with varying degrees of deformation are adjacent to each other with distinct boundaries. At both the outcrop and sample scales, clasts of quartz and feldspar, and white and black bands exhibit distinct structures. Based on microscopic observations, single-crystal quartz clasts showed undulatory extinction, suggesting subgrain boundary migration caused by dynamic recrystallization. Feldspar clasts contained inclusions with no regular arrangement, indicating that the clasts grew during the early stages of the deformation. Lens-shaped, elongated polycrystalline quartz clasts and fine-grained white bands composed mainly of quartz and feldspar exhibited grain boundary morphologies indicative of dynamic recrystallization through subgrain rotation (SGR).

Based on these observations and the inferred deformation mechanisms, the deformation processes of the shear zone were classified into six stages (Stages 0 to 5). This progressive sequence highlights the

transition from initial lithification to advanced deformation, governed by crystal growth of quartz and feldspar and competing dislocation creep. Shear localization into fine-grained bands is possibly attributed to the dominance of grain boundary sliding, which could be facilitated by fine-grained quartz and feldspar formed through grain size reduction during dynamic recrystallization.

Keywords: Subduction zone, Shimanto Belt, Shear zone, Ductile deformation

Deformation mechanisms and stress field induced by seamount subduction: A case study at Funafuseyama Unit, Mino belt

*Fuka Takuwa[1], Asuka Yamaguchi[1], Makoto Otsubo[2], Yusuke Shimura[2], Hanaya Okuda[3]

1. The University of Tokyo, 2. National Institute of Advanced Industrial Science and Technology, 3. Kochi Institute for Core Sample Research, Japan Agency for Marine-Earth Science and Technology

We focus on the relationship between seamount subduction and earthquakes in subduction zones. Geodetic and seismic observations indicate that large earthquakes are more likely to occur in regions where smooth seafloor subducts, whereas rough seafloor features may promote creep and slow slip (Wang & Bilek, 2014). A widely accepted model proposes that subducting seamounts induce plastic deformation in the overlying plate, creating complex fracture networks (Wang & Bilek, 2014). The role of fluid in this process is also emphasized (Sun et al., 2020; Chesley et al., 2021). However, compared to geophysical observations and modeling, geological studies remain limited, leaving significant gaps in our understanding of metamorphic and deformation processes, stress distribution, and their implications for earthquakes. This study aims to elucidate geological characteristics of an accreted seamount and its surrounding sedimentary facies, such as deformation mechanisms, temperature-pressure conditions, and stress distribution during accretion.

We investigated the Funafuseyama Unit of the Mino Belt in Gifu Prefecture, a Jurassic accretionary complex composed of mélanges with various-sized blocks of Permian chert, limestone, and basalt in a muddy matrix (Wakita, 2000). The limestone of shallow marine origin (Sano, 1988) and the basalt from plume activity (Ichiyama et al., 2008) suggest seamount accretion in this area. This study mainly focuses on Nukumitani as the main body of subducted seamount dominated by basalt, and compares it with Shirakuradani and Tarudani where chert and mélange are dominantly observed. In this study, we first created a route map and sketches of the outcrop at the bottom of basalt body. From samples, the chemical composition of cataclasite was analyzed using μXRF. Thin-section observations and μXRD analyses were performed for mineral identification. Furthermore, the stress inversion analysis (Yamaji, 2000) was also carried out using meso-scale faults and extension veins data collected from the geological survey. The maximum temperature for the muddy matrix was determined by Raman spectroscopy of carbonaceous material.

In Nukumitani, basalt outcrops were continuously observed, which corresponds to an approximately 1.3 km-thick seamount. At the basalt-mudstone boundary, a 48 m-thick shear zone was present with complex deformation structures of chert, limestone, basalt, and mudstone. We found minimal deformation for chert blocks, whereas basalt exhibited significant deformation and formed foliated cataclasite and fragmented structures. According to observations for polished slab and thin sections, pressure solution and cataclasis may accommodate deformation. These findings suggest that deformation during seamount accretion was concentrated at the basalt-mudstone boundary in the macroscopic scale. In a meter or smaller scales, shear strain is more concentrated within basalt and mudstone and less within chert and limestone.
The μXRD results revealed that the basalt in Nukumitani contains albite, oligoclase, chlorite, quartz, with absence of epidote or actinolite. Maximum temperature of muddy matrix indicate approximately 270C. Combining these results suggests that the basalt has experienced pressures less than 1 GPa.

Different stresses were detected in the Nukumitani and Shirakuradani/Tarudani. In Nukumitani, the stresses inferred from the faults have two distinct groups that may correspond to two different stress

stages. The stress from the mineral veins show that sigma1 is nearly vertical in both Nukumitani, Shirakuradani/Tarudani, while sigma2 and sigma3 are rotated about 30 degrees clockwise compared to Shirakuradani/Tarudani. These results indicate the variations in deformation stages or the presence of small-scale heterogeneities (less than 1 km), indicating localized stress fields. Additionally, the pore fluid pressure ratio in Nukumitani inferred from veins data is higher than one in Shirakuradani/Tarudani.

Keywords: Subduction Zone, Seamount

Frictional properties of limestone from seamounts under high temperature and high pressure

*Mayuko Sekikawa[1], Hanaya Okuda[2], Manami Kitamura[3], Miki Takahashi[3], Asuka Yamaguchi[4], Michiyo Sawai[1]

1. Chiba University, 2. Kochi Institute for Core Sample Research, Japan Agency for Marine-Earth Science and Technology, 3. National Institute of Advanced Industrial Science and Technology, 4. Atmosphere and Ocean Research Institute, The University of Tokyo

Earthquakes at a subduction plate interface are considered to occur due to the rupture of asperities. Topographic irregularity of subducted seafloor, such as seamount, is one of the factors influencing asperity formation. Seamounts are thought to generate large earthquakes by increasing the normal stress on the subduction interface (e.g., Cloos, 1992). On the other hand, they are also assumed to act as barriers for rupture propagation (e.g., Kodaira et al., 2000), or may promote creep or slow slip behavior (e.g., Mochizuki et al., 2008). Okuma et al. (2022) reveal that the friction on the surface of seamounts as well as the topographical influence contributes to forming geologically complex structures. Despite these numerous studies on subducting seamounts, systematic friction experiments focusing on subducting seamounts remain insufficient. This study aims to investigate the frictional properties of seamount-derived rocks and their relationship with earthquake generation through the experiments.

We used limestone sample collected from a Jurassic accreted seamount at the Funafuseyama Unit, the Mino Belt in Gifu Prefecture, Japan. Thin-section observations and X-ray diffraction analyses revealed that the limestone sample consists of calcite (98.2 wt%) and quartz (1.8 wt%).

Experiments were conducted using a gas-medium, high-temperature, high-pressure triaxial apparatus at AIST, at a confining pressure of 150 MPa, a pore pressure of 100 MPa, temperatures of 20-200˚C, and axial displacement rates of 0.1-100 μm/s. The steady state friction (μ_{ss}) ranged from 0.70 to 0.80 under all temperature conditions we investigated. The value of friction parameter (*a*-*b*) (rate dependence of μ_{ss}) depend significantly on temperatures: it decreases from positive (0.0023-0.0159) to neutral with increasing temperatures to 100˚C, then it becomes negative (-0.0012--0.0041) at temperatures higher than 150˚C.
The same trend of (*a*-*b*) was also observed in seamount-derived basalt (Sawai et al., 2024 JpGU). This suggests that a seamount may be a site of earthquake nucleation at depths with temperatures of >100˚C if limestone or basalt is present on a seamount at the plate boundary. In addition, since limestone has a higher strength (μ_{ss}: 0.70-0.80) than basalt (μ_{ss}: 0.39-0.55), basalt is more likely to undergo deformation than limestone when both lithologies coexist.

Keywords: Friction experiment, Subduction zone, Seamount, Limestone

Experimental investigation on effects of diagenesis on frictional and hydraulic properties of incoming sediments from Tohoku subduction zone

*Hayato Ito[1,2], Keishi Okazaki[1,2], Mizuki Ueda[1,3], Asuka Yamaguchi[4], Yohei Hamada[2]

1. Hiroshima University, 2. Kochi Institute for Core Sample Research, JAMSTEC, 3. University of Tsukuba, 4. AORI, The University of Tokyo

Slow earthquakes and earthquakes occur along the plate boundary of the Tohoku subduction zone. The plate boundary is thought to be composed of subducting sediments enriched in silica and clay minerals. Subduction progressively induces diagenesis in sediments at plate boundaries, leading to dehydration and lithification. Active dehydration of subducting sediments occurs at depths corresponding to the seismogenic zones of both slow earthquakes and earthquakes. Therefore, diagenesis of incoming sediments can significantly influence the mechanical properties of faults, potentially affecting the fault slip movement of plate boundary faults.
The friction experiments on sediments under hydrothermal conditions were performed using a gas-medium, high pressure-temperature triaxial deformation apparatus at Hiroshima University. The samples were collected from the outer-rise region of the Tohoku subduction zone, meaning that this sample has the potential to become a material composing the plate boundary fault at the seismogenic zone in a subduction zone in the future. Prior to the friction experiment, we conducted hydrothermal hot-press experiments on the incoming sediments to simulate diagenesis at a confining pressure of 150 MPa, a pore fluid pressure of 58 MPa, and temperatures ranging from 20℃ to 230℃, and running (cooking) durations of 10 minutes, 1 day, 1 week, and 1 month. After simulating diagenesis, friction experiments with velocity steps were conducted to obtain friction parameters of the rate- and state-dependent friction law.
During cooking, a logarithmic shortening of the sample thickness was observed. This indicates that time-dependent compaction and possibly reaction occurred during experiments. Friction coefficient of sediments from the Tohoku outer rise increased with increasing cooking time and temperature. The value of (a - b) decreased with temperature and with time. Velocity weakening (i.e., negative (a-b) value) was observed when the sample was heated at 100℃ for a week and at 150 ℃ for 10 minutes and 1 day. This condition corresponds to the shallow part of the seismogenic zone. These results indicate that sediments tend to transition from velocity-strengthening to velocity-weakening behavior as diagenesis progresses. This transition from velocity-strengthening to velocity-weakening will take for less than 10 minutes at the temperature above 150℃, for about a week at 100℃, for a few years at 60℃ and for 10 thousand years at 40℃.
These results suggest that long-term, low-temperature diagenetic processes on a geological timescale could induce the spectrum of fault slip behaviors such as steady slip, slow earthquakes and earthquakes

Keywords: Diagenesis, Slow earthquake, Frictional property, Rock deformation

Preliminary results of shear friction experiments using Shirahama sandstone for the construction of friction wear model

*Sumire Maeda[1], Futoshi Yamashita[2]

1. National Institute of Advanced Industrial Science and Technology, 2. National Research Institute for Earth Science and Disaster Resilience

It has been empirically demonstrated that the width of a fault damage zone correlates with the fault length and the cumulative displacement (e.g., Ogata, 1976; Otsuki, 1978). This empirical relationship has been used for evaluating the possible maximum magnitude of earthquakes on the fault. However, it has also been reported that the growth rate of the fault damage zone width relative to the cumulative fault displacement depends on the host rock type (Shipton et al., 2006). Furthermore, some faults were reported to deviate from this empirical correlation (Gomura fault zone, e.g., Matsuda et al., 2004). Therefore, elucidating the physical mechanisms behind this empirical correlation is important for understanding earthquake physics and assessing earthquake hazards. Hirose et al. (2012) conducted rotary shear experiments on calcareous sandstone and suggested that its low wear rate is related to the formation of fault mirror structures on the sliding surface. They also suggested that the low wear rate could account for the low growth rate of the fault zone width in the sandstone. Maeda et al. (2023, JpGU) also conducted rotary shear friction experiments on quartzose sandstone and found that the wear rate of quartzose sandstone is significantly low under the condition that the fault mirror structures are formed on the sliding surface. However, the mechanical conditions under which the fault mirror structures were formed were different for the calcareous sandstone and the quartzose sandstone, probably due to the difference in their mineral compositions. Since the mineral composition of the rock should be an important factor controlling the wearing processes, we investigated the friction and wear properties of Shirahama sandstone, which has a different mineral composition from the two sandstones mentioned above, by conducting the shear friction experiments. In this study, we report the preliminary results.
We prepared cylindrical specimens (diameter: 25 mm, length: 40 mm) from the Shirahama sandstone blocks collected from Wakayama Prefecture, Japan. Shirahama sandstone consists primarily of quartz (22.5%), plagioclase (29.9%), and matrix (36.7%), and is categorized as an arenitic sandstone (e.g., Fujita et al., 2000). All experiments were conducted using the rotary-shear friction apparatus at the National Research Institute for Earth Science and Disaster Resilience, under normal stresses of 0.5-1.2 MPa, equivalent slip velocities of 0.010-0.080 m/s, and slip distance up to approximately 50 m. In this study, we investigated the friction and wear properties against the input work rate (PV-value), which is defined as the product of the normal stress and the slip velocity. We considered the slip distances of 10-50 m to be the steady state and averaged the friction coefficient over that distance to use as a representative value, μ_{ave}. We also estimated two different wear rates based on axial shortening and the weight of the wear material collected after each experiment.
The results show that μ_{ave} transitions from higher values of 0.38–0.53 to lower values of 0.30–0.35 at the PV-value of 0.05 MW/m^2. The wear rate also exhibits a sudden increase at this critical PV-value. In addition, a ring-shaped fault mirror structure was observed on the sliding surface after the experiments with the PV-value higher than the critical value. This wear property of Shirahama sandstone contrasts with that of quartzose sandstone, whose wear rate remains very low under the conditions of the mirror structure formation (Maeda et al., 2023, JpGU). This inconsistency may also be due to differences in mineral composition.

Examination of development process of boundary shear in powdered quartz gouge by rotary-friction experiments

*Minoru Kudose[1], Tetsuro Hirono[1], Hatanaka Mamoru[2], Akito Tsutsumi[2], Takeshi Miyamoto[2], Satoshi Yukawa[3]

1. Osaka Metropolitan University, 2. Kyoto University, 3. Osaka University

Understanding the behavior of fault slip during earthquakes is extremely important for evaluating the amount of fault slip and estimating the energy released. In the process of faulting and increasing displacement due to shear of the subsurface rocks, plane structures with specific orientations such as Riedel and Y shear planes, develop. These are called composite planar fabric. Also, it is widely known that various foliation structures develop, not just the development of composite planar fabric, leading to thickening of shear zones. Furthermore, boundary shear is distinct from composite structures, with strain and displacement concentrated along either the hanging wall or the footwall. This has been reported through observations of internal fault structures in the field and observations of samples after friction experiments. (e.g., Marone and Scholz, 1989; Niemeijer et al. Niemeijer et al.). Numerical analysis of the shear deformation of granular materials has been conducted in previous studies, and the frictional behavior shows three stages of change ascending, descending, and steady state. Towards the end of the steady-state phase, a distinct discontinuous surface in particle velocity that correspond to boundary shear, was observed near the boundary between the gouge layer and the moving-side pressure plate. (Miyamoto et al.). However, the physical picture of the development of the boundary shear and its elementary processes are still largely unknown. Laboratory friction experiments and microstructure observations were conducted to elucidate the process of boundary shear development. Also, Numerical analysis will be conducted in parallel. In the laboratory rock friction experiments, a rotary friction tester installed at Kyoto University was used. In setting up the sample and experimental conditions, we attempted to eliminate scale effects by setting the value of the inertial number, a dimensionless quantity that qualitatively expresses the state of shear, to almost the same valueas (1e-4) in a previous study (Miyamoto et al., 2022). Specifically, artificial quartz sand with a grain size of 24.98 μm was used as the sample, with a slip velocity of 0.07 m/s and a vertical stress of 5 MPa. A sample of 2 g was used so that the thickness of the simulated fault gouge was approximately 1 mm at the start of the experiment. The maximum slip distance was 13 m. Thin sections of pre-compaction samples and samples at slip distances of 2, 6, and 13 m were prepared for observation of the deformed microstructure using a polarized light microscope. In parallel with the laboratory experiments, numerical analyses simulating the friction experiments were performed using the free software LIGGGHTS with a three-dimensional discrete element method. Measured values of Young's modulus and Poisson's ratio in quartz (Ohno et al., 2006) were set. A total of 1,700 particles with diameters of 1, 1.5, and 2 mm (average diameter 1.2 mm) were used, the slip velocity was set to 0.16 m/s, and the vertical stress was 25 MPa. The gouge thickness at the beginning of the analysis under vertical stress is approximately 17 mm. In the laboratory friction test, when slip distance was set to 13 m, localized grain refinement and discoloration were observed at the boundary surface, and this deformation was considered to correspond to a boundary shear. On the other hand, when slip distance was 2 m and the slipping was stopped just before the last sharp weakening, grain size reduction near the boundary was not observed, indicating a difference in the structure. The friction behavior of the slab decreased sharply when slip distance reached about 5 m, and remained almost constant at that low value. As a future plan, we confirmed something corresponding to boundary shear through thin section observation with a slip distance of 13m. To improve the accuracy of comparisons with numerical analysis, we will review the experimental conditions and conduct experiments under more

realistic conditions. In the presentation, we will report the preliminary results of the experiment and the results of the numerical analysis, and also the results of our investigation of the relationship between the development of the boundary shear, frictional behavior, slip distance, and time transition of the particle state.

Keywords: Friction experiment, Numerical analysis

Experimental evaluation of friction property of unaltered and altered basalt

*Yohei Donga[1], Minoru Kudose[1], Akito Tsutsumi[2], Tetsuro Hirono[1]

1. Osaka Metropolitan University, 2. Kyoto University

The quantitative evaluation of slip-on plate boundary faults during Nankai earthquakes is extremely important because it is directly related to the estimation of the size of the tsunami. Hirono et al. (2016) conducted diversified analyses and laboratory experiments using core samples collected from the Nankai Trough Megasplay fault off the coast of Kumano as the IODP Nankai Trough Seismogenic Zone Experiment, and the slip distance of 30-50 m was calculated through dynamic analysis. However, these results were obtained only from analytical and experimental values of clay samples collected from 271 m below the seafloor, and so this fault model does not reflect the oceanic plate stratigraphy. Therefore, we aim to quantitatively evaluate the peak friction coefficient, the dynamic friction coefficient, and Dc of distances from the start of the experiment to the steady state by our friction experiments using basalt, one of the representative components of the oceanic plate stratigraphy. In addition, considering the alteration of basalt at plate boundaries, we used two types of basalt in our friction experiments; unaltered basalt underlying the oceanic crust of the Cocos Plate and altered basalt exposed in the Mio Mélange of the Hidakagawa Group, Wakayama Prefecture, Japan. First, we ground the basalt samples with a mortar, obtained a specific grain size of 53-150 μm with a sieve, and did not dry samples. We held samples between two 25 mm diameter cylindrical blocks of gabbro, and covered the friction surface with a Teflon ring to prevent leakage of samples. Experiments were then conducted using a rotary-shear intermediate to high-velocity friction apparatus with a constant normal stress of 1.5 MPa, a slip velocity of 1 m/s, slip distances of 10 m, and a sample weight of 2 g. We obtained experimental results as follows. The unaltered basalt shows a peak friction coefficient of 1.00, a dynamic friction coefficient of 0.32, and Dc of 9.70 m. On the other hand, the altered basalt showed a peak friction coefficient of 0.88, a dynamic friction coefficient of 0.23, and Dc of 9.39 m. Comparing the values of the experiments for the two basalts, the altered basalt has the peak friction coefficient of 0.12 lower, the dynamic friction coefficient of 0.09 lower, and the Dc of 0.31 m shorter than those of the unaltered basalt. The powder X-ray diffraction analysis shows that the altered basalt contain more kaolinite and dolomite. This suggests that these minerals with lower strength formed by the alteration at the plate subduction boundary lead to the decrease in the friction coefficient of the basalt. As a future study, we will evaluate more comprehensive frictional properties of the unaltered and altered basalt by experiments at various constant normal stresses and with larger slip distances.

Keywords: Nankai earthquake, plate-subduction boundary, basalt, frictional property

Frictional behavior of cation-exchanged biotite

*Hanaya Okuda[1], Akiko Yamaguchi[2]

1. Kochi Institute for Core Sample Research, Japan Agency for Marine-Earth Science and Technology, 2. Center for Computational Science and e-Systems, Japan Atomic Energy Agency

Sheet silicates such as clay minerals play significant roles in deformation behavior of rocks due to their mechanical weakness. Cations on the sheet or in the layers are known to vary frictional strengths. Also, differences in crystal structures of sheet also have an influence on frictional strengths. This variety of frictional strengths of sheet silicates change the mechanical behavior of natural faults whose mineral compositions change with pressure and temperature conditions. Roles of the cations on/in the sheet and of the sheets themselves need to be separately understood because chemical composition of the sheet and its crystal structure change with diagenesis as well as cation species in natural systems.

In this study, we chemically weathered biotite using Na-TPB and EDTA and exchanged interlayer K into Na and water molecule (Kitayama et al., 2020; hereafter “Na-weathered biotite”). Friction experiments were performed on Na-weathered biotite as well as untreated biotite. We used an oil-medium triaxial deformation apparatus with direct shear assembly for the friction experiment. Effective normal stress and pore fluid pressure (with distilled water) of 20 and 10 MPa, respectively, were applied to the sample. Velocity step tests with 0.1-0.3-1-3 μm/s and slide-hold-slide tests with 30-100-300-1000-3000 seconds were performed.

Steady-state friction coefficients of Na-weathered biotite and original biotite were 0.18 and 0.40, respectively. The rate- and state-dependent friction (RSF) law parameter *a* were similar for both Na-weathered biotite and original biotite whereas Na-weathered biotite showed a smaller *b* than original biotite. The healing rate β was smaller for Na-weathered biotite than that for original biotite. Compared to cation-exchanged montmorillonite (e.g., Sakuma et al., 2022), this study shows a consistent trend that K-bearing sheet silicate has a higher frictional strength than Na-bearing sheet silicate. However, both Na-weathered biotite and original biotite showed higher friction coefficients than Na-montmorillonite and K-montmorillonite. This result indicates that both cations and chemical compositions of the sheet play roles in the frictional strengths of sheet silicate.

Keywords: Sheet silicate, Friction, Interlayer cation

Dependence of the rate- and state-dependent friction parameters of metagabbro gouge on normal stress

*Futoshi Yamashita[1], Kazuo Mizoguchi[2], Eiichi Fukuyama[3,1], Sachiko Iizuka[4]

1. National Research Institute for Earth Science and Disaster Resilience, 2. CRIEPI, 3. Graduate School of Engineering, Kyoto University, 4. CERES Inc.

The rate- and state-dependent friction (RSF) law can represent complex frictional slips and is widely used in simulations and modeling of various faulting behaviors. One of the friction parameters, the critical slip distance D_c, is recognized as the distance required for the transition to a new state after a change in the condition of the frictional contact. Laboratory experiments using rock powder as a simulated gouge have demonstrated a positive correlation between D_c and the thickness of the gouge layer or the shear band where the deformation is localized in it (Marone and Kilgore, 1993, Nature). Recently, Yamashita et al. (2024, SSJ meeting) reported that the D_c of metagabbro gouge appears to depend on the fault scale, based on the results of velocity step change experiments on centimeter- and meter-scale laboratory faults. They further suggested that the positive dependence of D_c on normal stress is one of the key factors causing the scale dependence of D_c. However, the normal stresses applied to investigate the normal stress dependence in their study were limited from 3.4 MPa to 20 MPa, leaving it unclear whether the positive dependence persists at higher normal stresses. In addition, for simplicity, only one state variable was assumed when estimating the friction parameters, which may be insufficient to understand the mechanism of the correlation, and a model with multiple state variables may be required. Therefore, we conducted velocity step experiments at higher normal stresses of 30 MPa and 40 MPa and estimated the RSF parameters assuming two state variables.

We used a biaxial friction apparatus at the Central Research Institute of Electric Power Industry (Mizoguchi et al., 2021, EPS), which is the same experimental apparatus as that used by Yamashita et al. (2024, SSJ meeting). The simulated gouge was also the same metagabbro powder (average grain size: 12 μm, maximum grain size: 75 μm), with an initial layer thickness of 3 mm. After applying a normal stress of either 30 MPa or 40 MPa, the velocity step changes were applied between 0.1-1.0-10.0-100.0 μm/s. The current analysis focused on the responses to the velocity increase steps from 10.0 μm/s to 100.0 μm/s and from 1.0 μm/s to 10.0 μm/s, which were identical or close to the conditions of the meter-scale experiments. Assuming that the responses follow the slip law (Ruina, 1983, JGR), the optimal combination of the friction parameters that can best reproduce the observed frictional behavior was determined using a grid search technique. To constrain the search space, we used available information directly from the experimental data: (1) approximating the system stiffness as the increase rate of friction coefficient to the displacement right after the velocity step, (2) determining the minimum value of the parameter a from the constraint that the peak friction coefficient after a velocity step from V_1 to V_2 does not exceed $a\ln(V_2/V_1)$, and (3) determining $(a\text{-}b_1\text{-}b_2)\ln(V_2/V_1)$ from the difference between the averaged friction coefficient right before the velocity step and that after the transient response after the step.

Examining the relationship between the normal stress and all friction parameters for the optimal model with a coefficient of determination R^2 greater than 0.5 for the experimental data, we found that $a\text{-}b_1\text{-}b_2$ decreases with increasing normal stress up to 10 MPa, beyond which it remains almost constant. Defining $D_{c1} < D_{c2}$, the average value of D_{c1} under all normal stress conditions is on the order of several micrometers, while D_{c2} has an average value of several hundred micrometers, both of which show no clear dependence on normal stress. However, focusing on the parameters for the velocity step from 10.0 μm/s to 100.0 μm/s, a, b_1, b_2 are almost constant independent of normal stress, while both D_{c1} and D_{c2} tend to increase with increasing normal stress up to 40 MPa. Since the loading rate in the meter-scale

experiments was greater than 10.0 μm/s, this normal stress dependence of D_c could become effective and then cause the scale dependence. We will continue to investigate the mechanisms from various aspects, such as observing the microstructures within the gouge layer.

Keywords: Friction experiment, Gouge, Rate and state dependent friction law, Normal stress dependence

Effects of pore fluid pressurization rate and permeability due to friction surface roughness on friction behaviors

*RIKU IWATA[1], SINICHI UEHARA[1]

1. TOHO university

The increase in pore pressure caused by fluid injection into deep underground formations for geothermal development poses a risk of inducing seismic slip. An increase in pore pressure on a fault plane reduces the effective normal stress and shear strength, thereby making the fault plane more susceptible to slip. The distribution of pore pressure on the fault plane correlates with the distribution of shear strength, potentially influencing the occurrence of injection-induced earthquakes. The distribution of pore pressure on a fault plane is expected to depend on the rate of pore pressurization during fluid injection (vp) and permeability along the fault plane. However, the effects of vp and permeability along the fault plane on frictional behavior remain unclear.
This study aims to elucidate the influence of the vp and fault surface permeability, which is associated with surface roughness, on frictional behavior though fluid injection friction experiments.

The rock sample was a cylindrical Aji granite specimen with a diameter of 40 mm and a length of 80 mm. This sample was cut at an angle at 30 degrees relative to the axial direction. To introduce pore fluid to the friction surface, a 2.5 mm diameter hole was drilled perpendicular to the friction surface, extending through the center of the bottom surface. To create friction surfaces with different permeabilities, the surfaces were polished with waterproof abrasive paper with two different grain size, #80 and #3000. Fluid injection experiments were conducted using a triaxial rock deformation apparatus. The main experimental conditions were a confining pressure of 60 MPa, an initial pore pressure of 0.1 MPa, and an axial loading rate of 0.1 mm/min. The experimental procedure involved maintaining a constant initial pore pressure and applying axial loading until a stick-slip and to keep the axial displacement was hold constant just before the next slip. Simultaneously, a syringe pump was used to control the pore pressure at constant vp. Two vp conditions were tested: vp = 0.1 MPa/min and 1.0 MPa/min. Downstream, the valve was closed, and the pore pressure was monitored using a downstream pore pressure gauge. Based on the experimental results, the effects of different vp and friction surface roughness on friction behavior were analyzed.

A comparison of the upstream pore pressure during slip in the vp = 0.1 MPa/min and vp = 1.0 MPa/min experiments on the #3000 specimens showed that, slip occurred at an upstream pore pressure of 6.9 MPa in the vp = 0.1 MPa/min experiment, and at 16.3 MPa in the vp = 1.0 MPa/min experiment. This indicates that the upstream pore pressure at the onset of slip was lower in the vp = 0.1 MPa/min experiment. This result is consistent with the findings of Passelegue et al. (2018) and is likely due to the more uniform distribution of pore pressure on the friction surface at lower vp. A comparison of the shear stress drop during slip revealed that, the vp = 0.1 MPa/min experiment resulted in a shear stress drop of 2.29 MPa, whereas the vp = 1.0 MPa/min experiment resulted in a shear stress drop of 3.30 MPa. The larger vp led to greater shear stress drop during slip, suggesting that the higher vp may result in larger seismic magnitude.
A comparison was made between the #80 and #3000 specimens in the vp = 1.0 MPa/min experiment. In the #80 sample, slip occurred at an upstream pore pressure of 24.6 MPa, whereas in the #3000 sample, slip occurred at 16.3 MPa. Thus, slip occurred at a higher upstream pore pressure in the #80 sample. It was initially expected that the #80 sample, which has higher permeability, would slip at a lower upstream

pore pressure because the pore pressure transmission to the friction surface. However, the experimental results deviated from this prediction. One possible explanation is that the friction surface of the #80 specimen was not sufficiently polished.

References

F.X. Passelegue, et al.,2018, Geophysical Research Letters,45,12,837-12,846.

Keywords: Injection-induced earthquake, Friction behaviors, Pore fluid pressure

Investigating Fracture Mechanisms in Hydraulic Fracturing by Dynamic Event Localization

*Zhi Yuan[1], Chen Gu[1], Yichen Zhong[1], Peng Wu[1], Zhuoyu Chen[1]

1. Tsinghua University

This paper presents a study investigating the fracture mechanisms through laboratory-scale hydraulic fracturing experiments. During the experiment, we monitored the acoustic emission (AE) signals of the fracturing process using a 24-sensor array, with four sensors placed on each surface of the sample cube-shaped shale specimen, containing a natural pre-existing fracture. A triaxial pressure system was used to apply confining stress, simulating real underground stress conditions. Fluid was injected through a central borehole, generating a fracture perpendicular to the pre-existing natural fracture.

By analyzing the recorded AE signals recorded by the sensor array during the experiment, we identified approximately 320 event signals. Each event was localized using NonLinLoc, an open-source nonlinear Bayesian localization software. Clustering the localized events allowed us to infer the evolution of fracture geometry and reconstruct the 3D velocity model revolution. We then performed the moment tensor inversion, incorporating velocity model variation, to analyze the source mechanisms of the events. Our results reveal a transition from dilatancy-dominant to shear-dominant mechanisms, offering new insights into the fluid-induced seismicity. These findings underscore the potential for dilatancy-based precursors in monitoring and early-warning systems for hydraulic fracturing-induced seismic events.

Keywords: Hydraulic-Fracturing, Event-Localization, Mechanism

Toward frictional experiments at brittle-plastic transition pressures with high-flux synchrotron X-ray

*Rikuto Honda[1], Tomoaki Kubo[1], Noriyoshi Tsujino[2], Yuji Higo[2], Sho Kakizawa[2], Sanae Koizumi[3], Yuta Goto[1]

1. Kyushu University, 2. JASRI, 3. The University of Tokyo

The frictional properties of rocks at the brittle-plastic transition (P ~1-2 GPa, depths of ~30-70 km) are crucial for understanding faulting processes in subduction zones. Multi-anvil deformation apparatuses can easily achieve high-pressure conditions and have been used to investigate faulting mechanisms by combining X-ray in-situ observations and acoustic emission (AE) measurements (e.g. Ohuchi et al., 2017; Honda et al., 2024). However, the time resolution of data acquisition was low (~10^{2} s) when using bending magnet X-ray sources (BM), making it difficult to capture detailed processes. Recently, advancements in high-resolution (~10^{-1} s) techniques have been made using high-flux insertion device X-ray sources (ID) (e.g. Ohuchi et al., 2024). In this study, we further developed these methods and applied them to examine the localization and frictional behavior of olivine under the brittle-plastic transition regime.

The experiments were conducted with D-DIA type apparatus at 1-5 GPa and 25-1040˚C, with in-situ observation using a 60 keV monochromatic X-ray from BM at SPring-8 BL04B1 and a 100 keV pink beam from ID at BL05XU and BL15XU. The starting material was sintered polycrystalline forsterite (Koizumi et al., 2010). It was processed into thin disks (~0.3 mm) and placed between alumina pistons which were saw-cut at a 45˚ angle to apply shear deformation. We carried out the deformation at a constant anvil displacement rate (0.2 mm/h) or with velocity stepping (0.2-2 mm/h). X-ray diffraction and radiography were measured to obtain pressure, stress-strain data, and localization behavior. The time resolution was 180-300 s with BM and 0.5 s with ID. Additionally, AE measurement was also conducted during the deformation to detect shear instability.

We first identified the variations in localization behaviors and their conditions using BM. We confirmed localization in all runs through radiography, except for the low-velocity deformation at highest temperature of 1040˚C. Unstable slips accompanied by AEs occurred only within a limited range of conditions below 2 GPa and at 150-710˚C, which is largely consistent with the conditions of earthquakes in warm slabs. Y-shear and Riedel shear planes developed after yielding, with the latter being particularly prominent in unstable slip involving AEs. Microstructural observation revealed the development of the fault gouge composed of submicron-sized particles, whose morphology varied with temperature. They had rounded shape and mylonitic texture at higher temperature, whereas they formed angular and cataclastic fracture structures at lower temperature. Furthermore, the yield stress exceeded the Goetze criterion (τ /P >0.5), suggesting that localization was initiated by brittle or semi-brittle crack formation. However, once faults formed, the strength decreased below that, transitioning to stable slip without AEs in some samples. In addition, even under identical conditions, variations in the friction coefficient and slip stability were observed, indicating that other factors, such as water content, must also be considered in these behaviors.

We also conducted velocity-step tests to examine the velocity dependence of the friction coefficient in unstable slips with ID. So far, we have successfully identified a trend of velocity weakening correlated with AE, localized deformation, and its onset. Nonetheless, challenges remain, including large measurement errors and stress variations due to changes in the diffraction acquisition position. While improving control

precision is necessary, the latter issue also suggests the possibility of capturing the stress distribution within the sample, which could potentially be evaluated quantitatively through high-resolution stress mapping. Although these types of experiments had been previously difficult using the BM method, high-resolution measurements with ID have enabled us to achieve them for the first time using multi-anvil apparatuses.

Keywords: brittle-plastic transition, high pressure experiments, friction, in-situ observation, insertion device X-ray source, acoustic emission

Earthquake Stress-Drop Estimation in Laboratory Experiment with Machine Learning

*Gauss Te-Chuan Chang[1,2], Chris Marone[3,4], Chun-Yu Ke[2]

1. Department of Physics, National Taiwan University, Taipei, Taiwan, 2. Department of Civil Engineering, National Taiwan University, Taipei, Taiwan, 3. Department of Earth Sciences, La Sapienza Università di Roma, Roma, Italy, 4. Department of Geosciences, Pennsylvania State University, PA, USA

Stress drop is a key parameter that influences earthquake rupture processes and ground-motion characteristics. By quantifying the difference in shear stress before and after a rupture, it offers direct insight into how energy is released during an earthquake. However, stress drop varies significantly from fault to fault and from event to event, underscoring the importance of improved measurement techniques. Previous studies have successfully adopted machine learning models in laboratory earthquake datasets to predict time to failure and shear stress. However, their experimental fault systems were predominantly unstable. Specifically, the system is unstable when the loading stiffness k' is much lower than the critical stiffness k_c', i.e., $k' \ll k_c'$. The single state variable rate-and-state friction model suggests that slow-slip behavior emerges in the special case where $k' \sim k_c'$, which has significance for slow earthquake detection and earthquake early-warning systems.

In this study, we conducted double direct shear experiments on granite faults and generated laboratory earthquakes across a range of critical stiffness ratios ($K = k'/k_c'$), from near-critical conditions ($K \sim 1$) to highly unstable ($K \ll 1$). These conditions were achieved by varying normal stress, shearing rate, and loading stiffness. Acoustic emission (AE) data were collected continuously at 2.5 MHz using an array of 12 ultrasonic piezoelectric transducers embedded in a steel block, which is in direct contact with one of the granite side blocks. Additionally, shear strain was recorded at 13 equidistant locations at 100 kHz to capture transient local strain perturbations along the 15-cm saw-cut granite fault. At near-critical conditions, we observed consecutive events with highly variable stress-drops. The datasets with diverse event characteristics better emulate natural faults without strictly repeating rupture patterns and offer a broader training set for machine learning models, enhancing robustness in stress drop estimation and potentially improving their ability to generalize across varying fault conditions.

For large earthquakes, well-established techniques—such as finite-fault inversions, back-projection, and other seismological models—can be used to estimate stress drop. However, for small earthquakes (magnitude M < 2), these methods often become infeasible due to sparse data and low signal-to-noise ratios. To date, accurately measuring the in-situ stress drop at small fault ruptures remains a challenge, and thus these techniques are typically evaluated through numerical simulations or laboratory analogs. Leveraging the power of Transformer-based machine learning, multiple acoustic emissions signals from different channels are concatenated into multi-dimensional features and fed into a Transformer model. By treating all these signals as one “multi-feature” sequence (rather than separate inputs), the self-attention mechanism within the Transformer can learn the complex temporal correlations among them. The model can effectively capture how changes in one signal relate to another over time, enabling robust predictions of stress drop even with limited, noisy data.

Our results confirmed that Transformer-based machine learning models can effectively estimate stress drop in laboratory earthquakes using AE data. The diverse dataset produced in our experiments better captures the variability seen in natural faults, making it more promising to apply ML models trained on laboratory data to real-world seismic events.

Keywords: Stress Drop, Earthquake Rupture Processes, Laboratory Earthquakes, Direct Shear Experiments, Machine Learning

